Nano Energy (2013) 2, 553–578

Available online at www.sciencedirect.com

ScienceDirect

journal homepage: www.elsevier.com/locate/nanoenergy

REVIEW

Recent progress in the development of anode and cathode catalysts for direct methanol fuel cells

Jitendra N. Tiwari[a,*], Rajanish N. Tiwari[b], Gyan Singh[c], Kwang S. Kim[a]

[a]*Center for Superfunctional Materials, Dept. of Chemistry, Pohang University of Science and Technology, San 31, Hyojadong, Namgu, Pohang 790-784, Korea*
[b]*Surface Science Laboratory, Toyota Technological Institute, 2-12-1 Hisakata Tempaku, Nagoya 468-8511, Japan*
[c]*Department of Biological Science and Technology, National Chiao Tung University, 1001 Ta Hsueh Road, Hsinchu, Taiwan, 300, R.O.C.*

Received 14 March 2013; received in revised form 18 June 2013; accepted 18 June 2013
Available online 3 July 2013

KEYWORDS
Methanol oxidation;
Oxygen reduction;
Anode catalysts;
Cathode catalysts;
Direct methanol fuel cell

Abstract
Continuous growth in global energy demand has sparked concerns about energy security and environmental sustainability. In the past two decades, attempts have been made in the development of innovative energy technologies. The direct methanol fuel cell (DMFC) is among the most promising alternative energy sources for the near future. Simple construction, compact design, high energy density and relatively high energy-conversion efficiency give the DMFC an advantage over other promising power sources in terms of portability. However, the translation of DMFCs into commercially successful products is precluded due to poor performance. In addition, low activity, poor durability and reliability and an expensive anode and cathode further discourage the application of DMFCs. In this regard, the present review article focuses on recent progress in the development of anode and cathode catalysts for DMFCs. The first part of the review discusses the *recent* developments in the synthesis of single-, double-, and multiple-component catalysts and new catalyst supports for anode electrodes. The section is followed by the chemical approaches employed to make alloys and composite catalysts, aiming to enhance their activity, reliability and durability for the methanol oxidation reaction. Finally, exciting new research that pushes the development of single-, double-, and multiple-component catalysts and new catalyst supports for cathode electrodes is introduced. In addition, size-, shape- and composition-dependent electrocatalysts that are advocated for methanol

*Corresponding author. Tel.: +82 54 279 2110; fax: +82 54 279 8137.
E-mail address: jnt_tiw123@yahoo.co.in (J.N. Tiwari).

2211-2855/$ - see front matter
http://dx.doi.org/10.1016/j.nanoen.2013.06.009

oxidation at the anode and oxygen reduction at the cathode are highlighted to illustrate the potential of the newly developed electrocatalysts for DMFC applications. Moreover, this article provides a comprehensive review of the experimental work that is devoted to understanding the fundamental problems and recent progress in the development of anode and cathode catalysts for DMFCs.

Contents

Introduction

Overview

Direct methanol fuel cells (DMFCs) have attracted considerable recent interest because of various advantages, including high power density, zero or low exhaust, ease of recharging, simple structure, and quick startup at low temperature [1–3]. However, one of the major drawbacks of the DMFC is its high manufacturing cost, which prevents their successful commercialization [3]. By initiating cost-effective steps from prototypes to mass production, manufacturing expenses can be reduced; however, the expensive materials required for the production of DMFCs remain a challenge because DMFCs operating at low temperature use platinum (Pt) and its alloys for the conversion of fuel at the anode and reduction of oxygen at the cathode. The high cost of Pt significantly increases the total price of the fuel cell devices. The problem can be solved in the short term by using single-, double-, and multiple-component catalysts and new catalyst supports. Therefore, the study of single-, double-, and multiple-component catalysts and new catalyst supports not only has emerged as a significant area of research and development but also has greatly influenced everyday life, as more products based on single-, double-, and multiple-component catalysts and new catalyst supports are increasingly introduced to the market. Extensive research in the past two decades has established that the physical and chemical properties of materials show significant changes if their dimensions are on the nanometer scale, which opens new avenues for a wide range of future applications [3,4]. Especially, physical properties of nanostructures, such as large surface area and novel size effects, markedly improve the efficiency of DMFCs [3,4]. Therefore, single-, double-, and multiple-component catalysts and new catalyst supports have become increasingly important in the development of DMFCs in recent years. In addition, there are two main types of effects that result from single-, double-, and multiple-component catalysts and new catalyst supports: (1) ‘trivial size effects’, which rely solely on the increased surface-to-volume ratio and decreased layer thickness and volume of the nanoparticles and (2) ‘true size effects’, which also involve changes in local material properties [5,6]. Therefore, nanoscale engineering of the material appears to be critical in the next stage of advancement of DMFCs. Development in recent years has shown that single-, double-, and multiple-component catalysts and new catalyst supports have great potential for innovative new technology for the recurring energy demand.

In this regard, the review article is mainly focused on recent developments in the field of DMFC anode and cathode catalysts; the role of single-, double-, and multiple-component catalysts and new catalyst supports for non-alloy and alloy nanoparticles is particularly discussed in more detail. In addition, challenges involved in the development of DMFCs and the reaction mechanism for

methanol oxidation and oxygen reduction are subsequently discussed in more detail.

The scope of this review

The review article briefly describes the principle of DMFC operation. Subsequently, challenges involved in DMFC anode and cathode electrocatalysts are described. In Section 3, a brief summary of the reaction mechanism for methanol oxidation is reported. Section 4 describes the reaction mechanism for oxygen reduction. Sections 5 and 6 address recent progress in the development of anode and cathode electrocatalysts for DMFCs. Sections 5 and 6 particularly focus on the role of single-, double-, and multiple-component catalysts and new catalyst supports with non-alloy and alloy nanoparticles in the development of highly efficient DMFCs. The final section will describe the conclusions. Some open problems and continuing challenges are also highlighted in the final section.

Direct methanol fuel cell (DMFC)

Principle of DMFC operation

The contemporary science and technology of DMFCs have already been extensively reported in many review papers and articles; interested readers can refer to references [7-9] for more details. In short, the main active components of a DMFC are the fuel electrode (anode), oxidant electrode (cathode), and an electrolyte sandwiched between them. Figure 1 shows the basic operational principle of a fuel cell with its reactant or product gases and ion conduction flow directions. A schematic drawing of the DMFC system is given in Figure 1, displaying the principle of DMFC operation. The DMFC converts chemical energy into electrical energy by oxidizing methanol to CO_2 and H_2O. A proton-conducting solid membrane, used both as an electrolyte and separator between anode and cathode, is sandwiched between porous structures (such as carbon). The latter serve both as current collectors and as a support for catalyst particles. Before catalyst deposition, the current collectors are impregnated with polymer electrolyte to provide intimate contact of the metal particles with both electron and proton conductors.

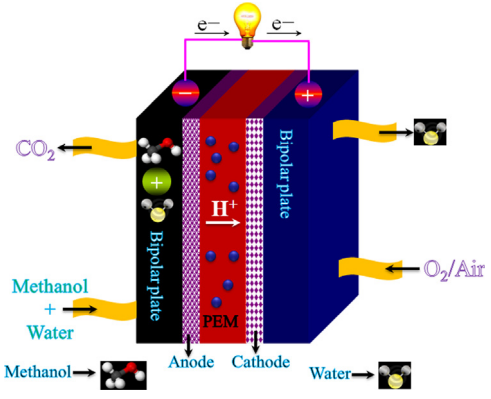

Figure 1 Schematic diagram of a DMFC. PEM=polymer electrolyte membrane.

At the anode, a methanol molecule reacts with an H_2O molecule and liberates CO_2, six protons that are free to migrate through the electrolyte towards the cathode and six electrons that can travel through the external load. The CO_2 produced in the reaction is rejected by the acid electrolyte solution. The protons migrating through the electrolyte and electrons moving *via* the external loaded circuit must reach a particle of catalyst on the cathode, where O_2 is electrocatalytically reduced and H_2O is produced. An electric potential occurs between the electrodes because of the excess of electrons at the anode (where they are generated) compared with the cathode (where they are consumed). This potential difference drives current through the external load, making the fuel cell a real source of power. The maximum theoretical voltage attainable from the overall reaction in the methanol-air fuel cell is ~1.21 V with a theoretical efficiency of 96.5%, but in practice, this voltage is not obtained due to poor electrode kinetics and ohmic losses in the electrolyte [10,11]. The relevant electrochemical reactions at the electrode surface in acidic media are [12] as follows:

Anode reaction: $CH_3OH+H_2O \rightarrow CO_2+6H^+ +6e^-$, $E_0=0.016$ V/SHE (1)

Cathode reaction: $3/2\ O2+6H^+ +6e^- \rightarrow 3H2O$, $E_0=1.229$ V/SHE (2)

Overall reaction: $CH_3OH+3/2O_2 \rightarrow CO_2+2H_2O$, $E_0=1.21$ V (3)

for which the standard hydrogen electrode (SHE) is used as a reference electrode.

Challenges

There are some crucial obstacles to overcome before large-scale commercialization of DMFC is achievable [13-15]: (a) the greatest present concern is the low activity and high cost of electrocatalysts in the anode and cathode; (b) the anode reaction has poor kinetics at lower temperatures, making identification of improved electrocatalysts and higher working temperatures highly desirable; (c) at the cathode, the oxygen reduction reaction is also slow: this problem is particularly serious with aqueous mineral acids, although studies show the issue is not quite as serious with acidic polymer membranes (Methanol vapor also appears in the cathode exhaust, from which it must be removed.); (d) the high cost of the currently used Nafion membrane (price=US$ 800-2000/m^2); (e) and the permeability of the current perfluorosulfonic acid membranes (Nafion, Figure 2) to methanol, which allows considerable crossover of methanol from the anode region to the cathode region. This crossover causes degradation of the performance of both electrodes, as mixed potential develops at the cathode, and deterioration of fuel utilization.

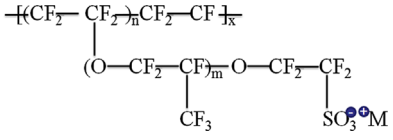

Figure 2 Chemical structure of Nafion, where n= 6.5−13.5; m=1, 2, 3...; x=200−1000; and M^+ is the exchangeable cation.

Reaction mechanism for methanol oxidation

Over the past several decades, materials scientists have sought to improve their knowledge of methanol oxidation mechanisms at different electrocatalysts under perfectly well-controlled conditions, such as different single crystal orientations and foreign metal clusters on polycrystalline or single crystal surfaces [10,16-18]. The basic mechanism for the methanol oxidation reaction (MOR) was first reviewed in 1988 [19]. Based on previous reports, the reaction can be summarized as follows [16-20]:

(1) Electrosorption of methanol.
(2) C–H bond activation (methanol dissociation).
(3) H_2O adsorption and activation.
(4) Addition of oxygen to adsorbed carbon-containing intermediates to generate CO_2, which can be facilitated by addition of a second metal in alloy systems.

The catalytic oxidation mechanism of methanol by Pt is schematically described in Figure 3. As shown in Figure 3, during the MOR, CO_{ads} is formed and strongly adsorbs onto the Pt electrocatalyst, reducing the surface area and thus the performance of the DMFC. Three reaction paths for methanol oxidation to CO_2 have been investigated to date. One is an indirect mechanism that involves a CO intermediate (path 1, Figure 3), and the other two are direct mechanisms in which methanol is oxidized to CO_2 without the formation of a CO intermediate (paths 2 and 3, Figure 3).

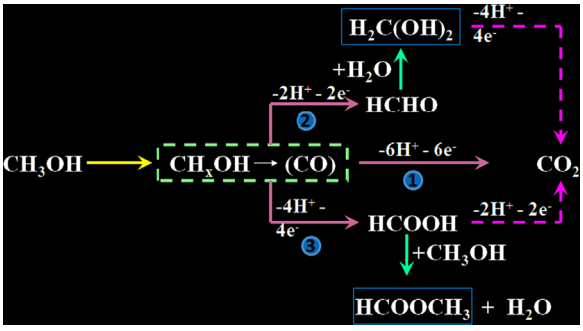

Figure 3 Schematic representation of the methanol oxidation reaction mechanism.

Reaction mechanism for oxygen reduction

The oxygen reduction reaction (ORR) is another important reaction in energy-converting systems such as DMFCs. However, the mechanism of the electrochemical ORR is very complicated and involves many intermediates. In addition, the ORR is highly dependent on the nature of the electrode material, catalyst, and electrolyte solution. The electrochemical reduction of O_2 in solution occurs by two main pathways: one involving the gain of two electrons to produce H_2O_2 and another producing H_2O by a direct four-electron pathway. The $2e^-$ and $4e^-$ reduction pathways in both acidic and alkaline media are given in Figure 4 [21-23]. To achieve maximum energy capacity, reduction of O_2 must occur via the $4e^-$ pathway. The four-electron reduction pathway is thus used in fuel cell systems; however, the two-electron reduction pathway is used in H_2O_2 production.

Anode catalysts of DMFCs

The success of DMFC technology depends on several factors, such as membrane, anode and cathode electrocatalysts. Among these, the anode electrocatalyst suffers from slow reaction kinetics that can only be overcome through developing new electrocatalyst types. With regard to new fuel cell anode electrocatalysts, there are two major concerns: performance, including activity, reliability and durability, and cost reduction. In the following section, recent progress in the development of DMFC anodes based on single-, double- and multiple-component catalysts is discussed in detail. In addition, a comprehensive overview of recently developed support materials for DMFC applications is covered.

Single-component catalysts

As a common catalyst for methanol oxidation, noble metals (such as Pt, Pd, and Au) can contribute significantly to DMFCs [24-27]. Therefore, a large variety of noble metal catalysts have been tested in DMFCs [24-27]. Reduced cost and improved methanol oxidation activity are especially desirable. The methanol oxidation activity of noble metal catalysts is strongly dependent on particle shape, size and surface structure [25]. Therefore, to increase methanol oxidation activity and reduce metal loading, many researchers have recently synthesized noble metal catalysts with different sizes, shapes and surface structures [25-27]. More recently, Lu et al. [26] synthesized ultrathin Au nanowires with high density stacking faults (HDSF) and studied their methanol oxidation properties in acidic and alkaline media.

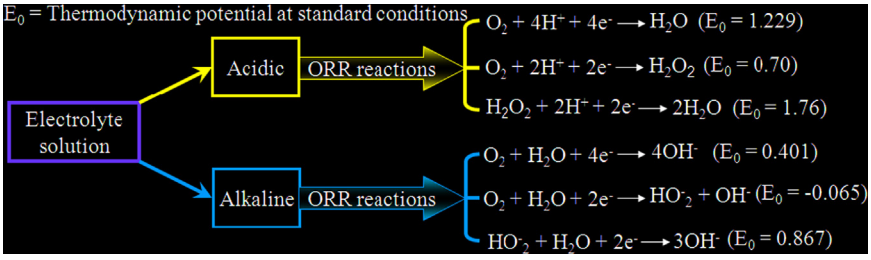

Figure 4 Schematic representation of the oxygen reduction reaction [21].

The ultrathin Au nanowires with an HDSF structure were synthesized from an Au precursor using oleylamine at 80 °C; in this reaction, oleylamine served as the solvent, reducing agent and surface capping agent. The Au nanowires exhibit higher electrocatalytic activity for methanol than do poly-Au nanoparticles and bulk Au in both acidic and alkaline media.

Generally, the MOR on an Au electrode proceeds in two distinct potential regions, with different mechanisms involving the two equations shown below: [28–30]

$$CH_3OH+5OH^- \rightarrow HCOO^-+4H_2O+4e^- \quad (4)$$

$$CH_3OH+8OH^- \rightarrow CO_3^{2-}+6H_2O+6e^- \quad (5)$$

At lower potentials, methanol was mainly oxidized to formates *via* an overall four-electron transfer reaction (Eq. 4). At higher potentials, the methanol molecules were oxidized to carbonates with the exchange of a six-electron transfer reaction (Eq. 5).

In 2009, Li et al. [31] fabricated Au nanoprism thin films on indium tin oxide (ITO)-coated glass substrates via wet chemical methods. The synthesized Au nanoprism thin films are single crystalline, whose basal and lateral surfaces are atomically flat {111} and {110} planes, respectively. The electrochemical catalytic activity of Au nanoprism thin films (Au surface modification with Pt) towards methanol oxidation was found to be much higher than that of commercial Pt-based catalysts due to the synergistic effect. Thus, even Au can exhibit high catalytic activity, but that performance is not sufficiently high for use in DMFCs. Therefore, researchers are looking for another metal. To overcome this problem, Wang et al. [32] synthesized nanoporous palladium rods and studied their electrochemical catalytic activity behavior in a methanol–KOH solution. The nanoporous palladium rods were fabricated through the chemical dealloying of rapidly solidified $Al_{80}Pd_{20}$ alloy in a 5 wt% HCl aqueous solution under free corrosion conditions. Individual nanoporous palladium rods were several microns in length and several hundred nanometers in diameter. In addition, all nanoporous palladium rods had a three-dimensional (3D) bicontinuous interpenetrating ligament-channel structure with a length scale of 15–20 nm. Moreover, the nanoporous palladium rods with high specific surface areas revealed superior electrocatalytic performance (223.52 mA mg^{-1}) toward methanol oxidation in alkaline media [32]. Recent investigations showed that Pt nanoparticles are more promising electrocatalysts than Pd and Au nanoparticles for the DMFC anode [33-42]. Nevertheless, one of the most important goals in nanoparticle-based electrochemistry is to understand how electrocatalytic activity is influenced by surface structure and nanoparticle shape [35]. In this regard, we first discuss the reported electrocatalytic properties of shape-controlled nanoparticles. Han et al. [36] synthesized Pt nanocube catalysts approximately 3.6 nm in size by a polyol process in the presence of polyvinylpyrrolidone (PVP) as a stabilizer and Fe^{3+} ions as a kinetic controller. The Pt nanocubes were single-crystalline with exposed (100) planes. These Pt nanocube catalysts showed a lower onset potential and higher current density for methanol oxidation than polycrystalline Pt. In addition, Han et al. found that the edge of the stepped (100) planes in the Pt nanocube catalyst was more preferable for the easy breaking of the methanol C–C bond than polycrystalline Pt. Recently, Lee et al. [37] reported Pt nanocubes ~4.5 nm in size that were synthesized by a modified polyol method with the assistance of a thermal reduction process. These Pt nanocubes with well-defined (100) planes provided much higher electrocatalytic activity toward the MOR than the spherical Pt/C with a polycrystalline structure. The excellent electrocatalytic activity of Pt nanocubes for the MOR may be due to predominantly exposed (100) planes. More recently, our group also reported the synthesis of shape-controlled perfect Pt nanoparticles via a pair of low-resistivity fastened silicon (FS) wafers at room temperature [38]. We also found that perfect Pt nanocubes deposited on FS wafers exhibited much higher electrocatalytic activity and stability for methanol oxidation than truncated Pt nanocubes, truncated Pt (cubes-tetrahedra) or spherical Pt nanoparticles. We reported that the high electrocatalytic activity of perfect Pt nanocubes is mainly due to the exposed Pt (100) planes of the single crystals. Liang et al. [41] synthesized Pt hollow nanospheres on a large scale via a replacement reaction between Co nanoparticles and H_2PtCl_6. From electrocatalytic calculations, the electrocatalytic activity of the Pt hollow nanospheres was twice that of the solid Pt nanoclusters. The high methanol oxidation current of the hollow-sphere catalysts was directly related to their high surface area. In addition, the incomplete shell of a hollow nanosphere may provide an interior surface for the electrocatalytic reaction. Liang et al. reported that the inner and outer surfaces of a hollow nanosphere can participate in the electrocatalytic reaction. Although Pt nanocubes and Pt hollow nanospheres have high electrocatalytic activity and stability, they suffer from a smaller electroactive surface area (ESA). Therefore, our group fabricated a two-dimensional (2D) continuous Pt island network by electrochemical deposition on a flat silicon substrate [40]. The ESA of this 2D continuous Pt island network was 67 $m^2\ g^{-1}$, which is much higher than that of a Ru-decorated Pt film electrode (21 $m^2\ g^{-1}$) and a blanket Pt electrode (16 $m^2\ g^{-1}$). The 2D continuous Pt island network exhibited higher CO and methanol oxidation activities than did the Ru-decorated Pt film and blanket Pt electrodes. The improvement of the CO and methanol oxidation activities can be attributed to the synergistic effect of the Pt island catalyst and the SiO_2 surface layer. In an endeavor to produce 3D nanostructured materials for DMFCs [33], our group synthesized 3D Pt nanoflowers that had a higher surface area than that of the Pt thin film/Si electrode. Moreover, compared to blanket Pt thin films, 3D Pt nanoflowers/Si had much higher electrocatalytic activity, with a steady-state current density approximately 310 times higher than that of the thin film Pt/Si electrode. The electrochemical characteristic curves of 3D Pt nanoflowers and blanket Pt thin films were obtained in 1 M H_2SO_4–1 M methanol (Figure 5) [33]. The anodic peak in the reverse scan can be attributed to the removal of incompletely oxidized carbonaceous species (CO-like species) formed in the forward scan. Thus, the ratio of the forward anodic peak current density (I_f) to the backward anodic peak current density (I_b), I_f/I_b, can be used to describe the CO tolerance of a catalyst to accumulation of carbonaceous species [33,40]. A low I_f/I_b indicates poor oxidation of methanol to CO_2 during the forward anodic scan and excessive

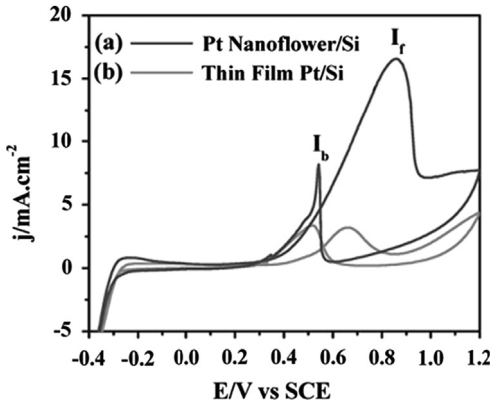

Figure 5 CV curves of 3D Pt nanoflowers/Si and thin film Pt/Si in a solution of 1 M CH_3OH-1M H_2SO_4 [33]. Reprinted by permission of the Royal Society of Chemistry.

accumulation of carbonaceous residues on the catalyst surface. However, high I_f/I_b indicates excellent oxidation of methanol during the forward anodic scan and less accumulation of residue on the catalyst. As shown in Figure 5, the I_f/I_b ratio of 3D Pt nanoflowers (~2.5) is higher than that of Pt thin film (~0.93), indicating less accumulation of CO-like species on the catalyst during the MOR and thus excellent catalytic activity.

Other groups also reported the effectiveness of 3D nanostructured materials on electrocatalytic properties [34,42]. More recently, Rauber et al. [42] synthesized highly ordered 3D Pt nanowire networks by a method based on hard templates using electrodeposition within nanochannels of ion track-etched polymer membranes. The network structures consisted of well-defined interconnected nanowires with controlled morphologies and compositions. The electrocatalytic activity of the 3D Pt nanowire networks in the MOR was measured in H_2SO_4 (0.5 M) and methanol (0.5 M) at room temperature. The peak current densities of the anodic peaks of 3D Pt nanowire networks, PtB, and Pt/C catalysts were 0.76, 0.39, and 0.24 mA/cm^2, respectively, showing the high electrocatalytic activity of 3D Pt nanowire networks. The excellent electrocatalytic activity is a direct consequence of the inherent properties of the continuously organized, porous 3D architecture, resulting in excellent transport properties and efficient access of the reactants to catalytic sites. Anode poisoning by the intermediates or CO-like species formed during the MOR on Pt catalysts is a familiar phenomenon. In addition, due to the high cost, commercial applications of noble Pt metal catalysts have been restricted. However, the modification of Pt catalysts with other metals or metal oxides that have higher tendencies to form surface oxygenated species at lower potentials is one of the best methods to solve this problem [43,44].

Double-component catalysts

Another major problem for the efficient conversion of methanol fuel to electric current in a DMFC is the sluggish MOR kinetics on the anode catalyst. This slow nature is mostly due to self-poisoning of the surface by reaction intermediates such as CO_{ads}-like species that are generated during the stepwise dehydrogenation of methanol [45-48]. Therefore, the MOR on Pt is possible only at potentials where adsorbed CO_{ads}-like species and other poisoning intermediates are effectively oxidized, leading to significant overpotential and loss in DMFC efficiency [49]. This problem necessitates the search for binary Pt-based alloy (double-component) catalysts, such as PtRu [50,51], PtSn [52,53], PdNi [54], PtMo [55,56], $PtTiO_2$ [57,58], PtW [55], PtOs [60], and PtMn [61]. These alloyed metals can provide OH species at more negative electrode potentials to react with CO_{ads}-like poisoning species, thus improving the electro-oxidation activities of methanol. Zhang et al. [62] deposited Pt nanoparticles on a nanoporous Au substrate by a simple immersion-electrodeposition technique, forming porous nanostructured Pt-Au catalysts. These porous Pt-Au catalysts have better electrochemical activity, antipoisoning ability, and long-term structural stability than commercial Pt-Ru catalysts, which can be justified by the bifunctional mechanism of bimetallic catalysts. According to the bifunctional mechanism, the oxidation of surface CO_{ads} species at the bimetallic porous Pt-Au catalysts would proceed through one of the following three routes:

$$Pt\text{-}CO_{ad}+Au\text{-}OH_{ad} \rightarrow CO_2+H^+ +Pt+Au+e^- \quad (6)$$

$$Au\text{-}CO_{ad}+Au\text{-}OH_{ad} \rightarrow CO_2+H^+ +Au+e^- \quad (7)$$

$$Pt\text{-}CO_{ad}+Pt\text{-}OH_{ad} \rightarrow CO_2+H^+ +Pt+e^- \quad (8)$$

Wang et al. [63] investigated the MOR activity on an Au-modified Pt (Au/Pt) electrode together with phosphomolybdic acid. In the typical synthesis of the Au/Pt electrode, the first step required forming an underpotential deposition (upd) Cu adlayer on the Pt substrate; the upd-Cu adlayer was then replaced by Au from $HAuCl_4$ aqueous solution. This replacement process takes place by the following reaction:

$$3upd\text{-}Cu/Pt+2AuCl_4^- = 2Au/Pt+3Cu^{2+}+8Cl^+ \quad (9)$$

Further, the performance of Au-modified Pt as a catalyst for the MOR was investigated by Wang et al. [62]. Analysis of data indicated that the MOR on Au-modified Pt was markedly enhanced not only by phosphomolybdic acid solution but also by adatom Au. The authors reported that adsorbed hydrogen and intermediate CO from methanol dehydrogenation and oxidation were electrocatalytically oxidized by the oxidant state of phosphomolybdic acid in the presence of an Au catalyst. To improve activity and stability, Zhang et al. [64] fabricated a novel nanoporous bimetallic Pt-Au alloy nanocomposite by dealloying the rapidly solidified $Al_{75}Pt_{15}Au_{10}$ alloy in NaOH or HCl aqueous solution. The dealloying leads to the formation of nanoporous $Pt_{60}Au_{40}$ nanocomposites. This electrode showed superior catalytic activity towards the MOR in acidic media compared to the commercial JM-Pt/C catalyst. Lee et al. [65] more recently synthesized octahedral Pt-Pd nanoparticles by means of a polyol process with glycerol as a reducing agent. The dominant exposed surfaces of the octahedral Pt-Pd nanoparticles were (111) facets, with well-defined alloy formation between the Pt and Pd metallic phases. According to their analysis, the octahedral Pt-Pd alloy catalysts showed improved specific activity and long term stability compared to polycrystalline Pt/C in the MOR. Other researchers have also reported that Pt and Pd electrodes with (111) facets

exhibited lower onset potentials and higher current densities for methanol than electrodes with other low-index facets [66]. Jiang et al. [67] made bimetallic Pt_mNi_n electrocatalysts with different Pt/Ni atomic ratios through a polyol process. Briefly, $H_2PtCl_6 \cdot 6H_2O$ and $Ni(NO_3)_2 \cdot 6H_2O$ were first mixed in 1 M NaOH/ethylene glycol solution and further stirred for 0.5 h to obtain the homogeneous solution. The metal salts were reduced by EG through heating of the homogeneous solution in an oil bath at 180 °C for 4 h in the presence of N_2 gas. The resulting product was subsequently filtered and washed with a large amount of distilled water. The amounts of the metal (Pt and Ni) precursors were adjusted to maintain the atomic ratios of Pt and Ni. Moreover, due to charge transfer from Ni to Pt atoms in Pt_mNi_n clusters, bimetallic Pt_mNi_n electrocatalysts exhibited enhanced activities for the MOR and decreased CO adsorption in alkaline media.

More recently, Qi et al. [54] fabricated a $Pd_{40}Ni_{60}$ alloy catalyst by applying an approach similar to that of Zhang et al. [64]. The $Pd_{40}Ni_{60}$ alloy consists of nanocrystals with sizes of 5–10 nm, and nanocrystalline and amorphous zones and lattice distortion were observed in the $Pd_{40}Ni_{60}$ alloy. The authors reported that $Pd_{40}Ni_{60}$ alloy had enhanced electrocatalytic performance towards the MOR in alkaline media than nanoporous Pd. This enhanced electrocatalytic activity is due to the following reasons: (1) the electronegativity of Pd (2.20) is larger than that of Ni (1.91), thus the transfer of electrons from Ni to Pd may occur, which can decrease the Pd–CO binding energy, improve CO oxidation from methanol dehydrogenation, and enhance the adsorption and oxidation of methanol molecules. In addition, like Ru, Ni is an oxophilic element and has the capacity to generate OH_{ads} at a lower potential and facilitates the oxidative desorption of the intermediate products, thus enhancing both the catalytic activity and stability of Pd catalysts [68].

Recently, core–shell nanoparticles have attracted extensive attention in materials science because of their many unique physical/chemical properties relative to their single-component counterparts, such as monodispersity, stability, maneuverability, and self-assembly. Long et al. [69] have recently synthesized Pt–Pd core–shell structures by a modified polyol method with the assistance of $AgNO_3$. Their cyclic voltammetry results showed that Pt–Pd core–shell structures had excellent electrocatalytic activities compared with alloy nanoparticles as well as mixed nanoparticles of various single and bimetallic components. Khalid et al. [70] also synthesized bimetallic core–shell Au–Pt nanoparticle assemblies on silicon and ITO-coated glass substrates. Core–shell Au–Pt nanoparticles were synthesized by the simultaneous reduction of surface-bound $[AuCl_4]^-$ and $[PtCl_6]^{2-}$ ions. In this process, Pt was first reduced to Pt^{2+} from Pt^{4+} and then to Pt^0, with standard redox potentials of 0.775 V for $[PtCl_6]^{2-}/[PtCl_4]^{2-}$ and 0.68 V for $[PtCl_4]^{2-}/Pt^0$, compared to a single-step reduction for gold from Au^{3+} to Au^0, with a standard reduction potential of 1.002 V for $[AuCl_4]^-/Au^0$ [71]. On the basis of reduction potentials, Au will preferably nucleate first to form the core, followed by Pt to form the shell. Such core–shell structures exhibited enhanced MOR activity, which was attributed to the electronic effect of the Au core Au on the Pt shell. Long et al. [69] prepared shape-controlled Pt–Pd core–shell bimetallic nanoparticles by a modified polyol process with the assistance of $AgNO_3$. In the case of epitaxial growth, the overgrowth of Pd shells on Pt cores was observed, but the overgrowth of the Pt shell on Pd cores was non-epitaxial growth. The size range of Pd–Pt core–shell nanoparticles was ~18–25 nm. Based on electrochemical measurements, the Pt–Pd core–shell (15 min) catalyst showed more enhanced activity than a Pt–Pd alloy and cluster for the oxidation of methanol. Long et al. reported that Pt–Pd core–shell (15 min) nanoparticles showed higher MOR activity due to their unique structure (shells as atomic monolayers on the cores) and homogeneous size. Ghosh et al. [73] prepared a Pt—Cd alloy by coreduction of K_2PtCl_6 and $CdCl_2$ with $NaBH_4$ in 1:1 ratio and annealing at 300 °C. The Pt—Cd nanoparticles showed much higher MOR activity than Pt due to the presence of the PtCd tetragonal ordered intermetallic phase. Xing et al. deposited Pt nanoparticles onto TiO_2 nanotubes (Pt/TiO_2NTs) by cyclic voltammetry [58]. The TiO_2NT arrays were fabricated by potentiostatic anodization of the Ti foil. The Pt/TiO_2NTs catalyst exhibited better electrocatalytic activity and stability toward the MOR due to the increase in the oxophilicity of TiO_2NTs. More recently, Shi et al. [74] also prepared Pt/$Ca_\delta TiO_x$-Ti_2O (Pt/TCT) catalysts by chemical methods. The nano- and submicro-sized Ti_2O and $Ca_\delta TiO_x$ were produced by partial metallization of TiO_2 nanoparticles

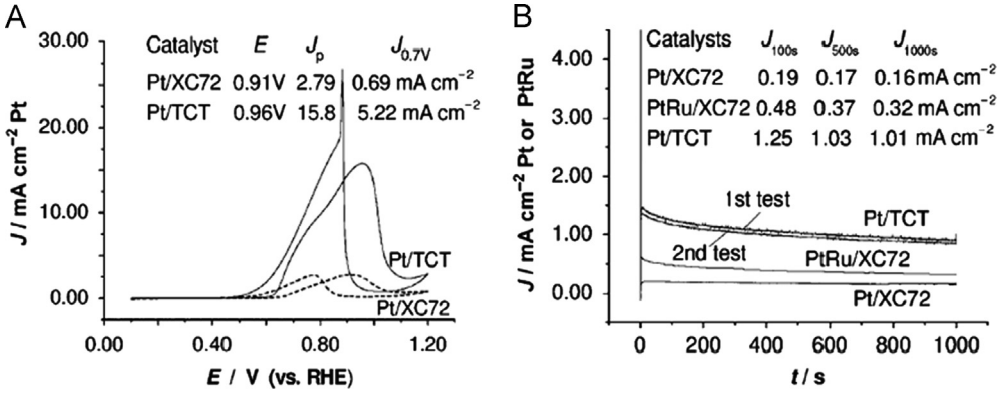

Figure 6 (A) CV curves of Pt/XC72 (dashed line) and Pt/TCT (solid line) in a solution of 1 M CH_3OH – 0.5 M H_2SO_4 at 60 °C; (B) Chronoamperometry curves of Pt/TCT (first and second tests on the same catalyst), Pt/XC72 and PtRu/XC72 catalysts in a solution of 1 M CH_3OH – 0.5 M H_2SO_4 at 0.6 V and 60 °C [74]. Reprinted by permission of the Wiley-VCH Verlag GmbH & Co. KGaA.

and an eutectic mixture of $CaCl_2$ and NaCl at 600 °C. Based on the CV results, Pt/TCT catalysts showed an oxidation peak current that is ~7.5-fold greater than that of Pt/XC72 (Figure 6 (A)). In addition, the chronoamperometric results also exhibited that Pt/TCT had higher catalytic activity for the MOR at 0.6 V (Figure 6 (B)). Electronic and bifunctional effects affected the comparable catalytic activities of $Ca_\delta TiO_x$ and Ti_2O in partially electrometallized TiO_2.

Kang et al. fabricated Mn—Pt nanocubes from Pt acetylacetonate and manganese carbonyl in the presence of oleic acid and oleylamine [61]. The structure of the as-synthesized Mn—Pt nanocubes was converted to an ordered $MnPt_3$ intermetallic phase after annealing at 600 °C. According to their data, the Mn—Pt nanocubes exhibited higher MOR activity than ETEK Pt and spherical Mn—Pt nanoparticles. Wang et al. [76] synthesized Pt-on-Pd nanodendrites by spontaneous step-by-step depositions of Pd and Pt precursors in the absence of Pd seeds, organic solvent, or high temperature. The CV curves indicated that the current densities of Pt-on-Pd nanodendrites were higher than those of Pt nanodendrites and Pt black. Such a nanodendrite structure was very favorable for reduction of the electronic binding energy in Pt and facilitation of the C–H cleavage reaction in methanol decomposition. Thus, Pt-on-Pd nanodendrites showed superior MOR activity. Cui et al. [77] reported the synthesis of porous Pt–Ni nanoparticle tubes for the electrocatalytic oxidation of methanol. The porous Pt–Ni nanoparticle tubes were synthesized by thermally annealing the AAO template-supported Pt–Ni nanoparticle tubes. This porous catalyst exhibited high catalytic activity, improved stability and high resistance to CO poisoning due to compressive strain.

Magnetic materials such as Pt–Co have been used as an ORR [78], but their suitability as a DMFC anode catalyst has not been explored in great detail. Zeng et al. [48] synthesized carbon-supported Pt–Co and Pt catalysts by $NaBH_4$ reduction of metal precursors. The authors found that the size of nanoparticles changed with the pH; for example, the size of nanoparticles in an alkaline medium was ~12 nm, while the size of nanoparticles in un-buffered solution was ~3.7 nm. They also found that Pt-Co nanoparticle catalysts were more active than Pt-only catalysts in acidic media and that the increase in specific activity was more than a surface-area effect. They believed that oxophilic Co acts as a catalyst promoter. Recently, Yang et al. [80] prepared high-quality and (100)-facet-terminated Pt_3Co and Pt nanocubes in the presence of oleylamine, oleic acid and argon gas. Figures. 7 (A, C and B, D) exhibited TEM and HRTEM images of the Pt_3Co and Pt nanocubes. The catalytic activity of (100)-facet-terminated Pt_3Co nanocubes towards the MOR was found to be much higher than that of Pt nanocubes, which was attributed to weaker and slower CO adsorption.

Among the various types of double-component catalysts, the Pt–Ru alloy has been found to be the most active and is the state-of-the-art anode catalyst for DMFCs. The enhanced catalytic activity and improved CO tolerance of the Pt–Ru catalyst relative to Pt for CO and methanol oxidation has been ascribed to both a bifunctional mechanism [81] and a ligand (electronic) effect [82]. Peng et al. [83] synthesized 3D nanoporous Pt–Ru bimetallic networks by decorating nanoporous Pt networks with Ru using a hydrothermal process. Further, a CV curve was used to characterize the electrochemical properties of synthesized nanoporous Pt–Ru networks. The CV curves of a Pt electrode, nanoporous Pt and nanoporous Pt–Ru are exhibited in Figures 8(A) and (B). As shown in Figures 8(A) and (B), nanoporous Pt–Ru significantly enhanced the ECSA and MOR activity and reduced the onset potential.

Yoo et al. [51] fabricated multilayered Pt/Ru nanorods with controllable bimetallic sites by the oblique angle deposition (OAD) technique. They synthesized single-segmented Pt nanorods and multi-segmented PtRu nanorods with 3, 7, and 13 layers via OAD. The electrochemical results suggest that the MOR over 13-layered PtRu nanorods shows enhanced catalytic activity compared to CeO_2 7-layered PtRu nanorods, 3-layered PtRu nanorods and Pt nanorods. The enhanced catalytic activity can be attributed to the electronic effect, which promotes the weakening of the bond of a CO-like species. In addition, the catalytic performance of 13-layered PtRu nanorods was also affected by the number of bimetallic pair sites, degree of alloying, and *d*-band vacancy. More recently, Şen et al. [85] fabricated carbon-supported PtRu nanoparticles (Ru/Pt: 0.25) by three different reduction processes: simultaneous reduction of $PtCl_4$ and $RuCl_3$ (catalyst A) and changing the reduction order of $PtCl_4$ and $RuCl_3$ (catalysts B and C). Their results suggest that catalyst C had better tolerance to CO poisoning than catalysts A and B. Moreover, catalyst C displayed superior performance relative to catalysts A and B in terms of catalytic activity and stability. Although double-component catalysts such as Pt–Ru exhibited better CO-tolerance and higher MOR activity in acidic and alkaline media, the commercial viability of DMFCs remains hindered due to the high costs (Pt–Ru catalysts) and low abundance of

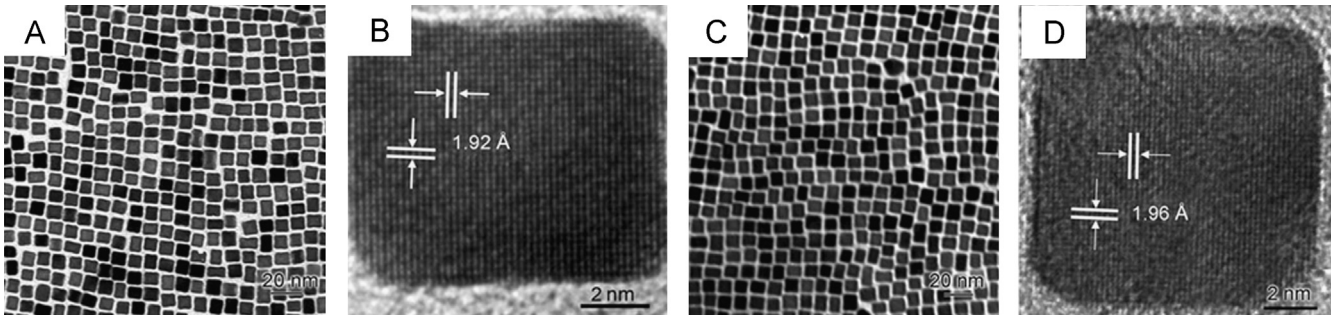

Figure. 7 (A) TEM and (B) HRTEM images of Pt_3Co nanocubes; (C) TEM and (D) HRTEM images of Pt nanocubes [76]. Reprinted by permission of the Wiley-VCH Verlag GmbH & Co. KGaA.

noble metal catalysts. Furthermore, the supply of Ru and the CO poisoning effect of Ru remain questionable. The research for a low-cost, durable and more active catalyst for the MOR in acidic and alkaline medium is thus of great importance.

Multiple-component catalysts

As discussed previously, we found that the addition of Ru has proven effective in improving anti-poisoning performance. However, the high cost of the Pt-Ru catalyst is also one of the main obstacles to its scaled application [86]. The wide commercialization of DMFCs mainly depends on decreasing the cost of the catalysts [87]. The above-mentioned problems can be solved by modifying Pt catalysts with other metals or metal oxides that have higher tendencies to form surface-oxygenated species at lower potentials. To this end, serious efforts have been made by several groups to synthesize new catalyst systems for methanol oxidation based on multiple-component catalysts such as PtRuNi [88-90], PtRuMo [89,91,92], and PtMOx (M=Ti, V, Mn, W) [93-96]. Wang et al. [92] prepared a PtRuMo catalyst by an impregnation reduction process. In the synthesis of the PtRuMo catalyst, sodium borohydride was used to chemically reduce the precursors of H_2PtCl_6, $RuCl_3$ and $(NH_4)_6Mo_7O_{24}$, in different atomic ratios. The authors found

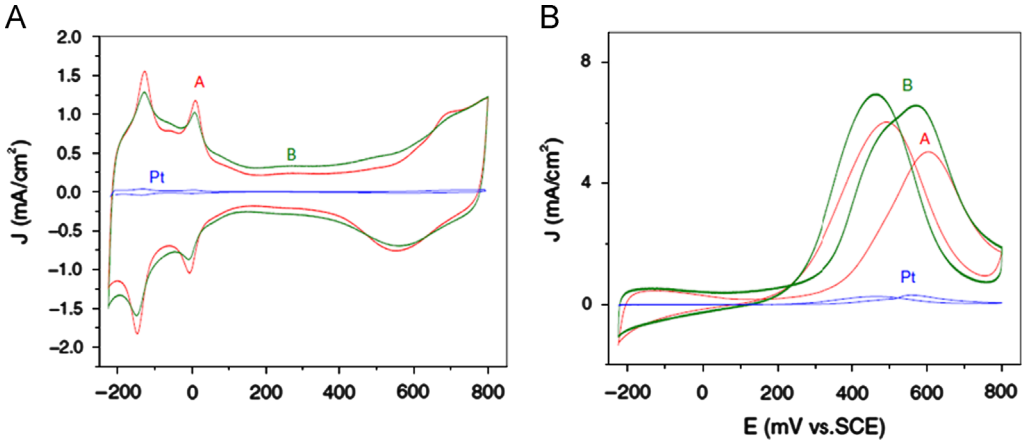

Figure. 8 CV curves of polycrystalline Pt electrode, nanoporous Pt (A) and Pt-Ru (B): (a) in 0.5 M H_2SO_4 at 20 mV s^{-1}; and (b) in 0.1 M CH_3OH-0.5 M H_2SO_4 at 20 mV s^{-1} [83]. Reprinted by permission of IOP Publishing Ltd.

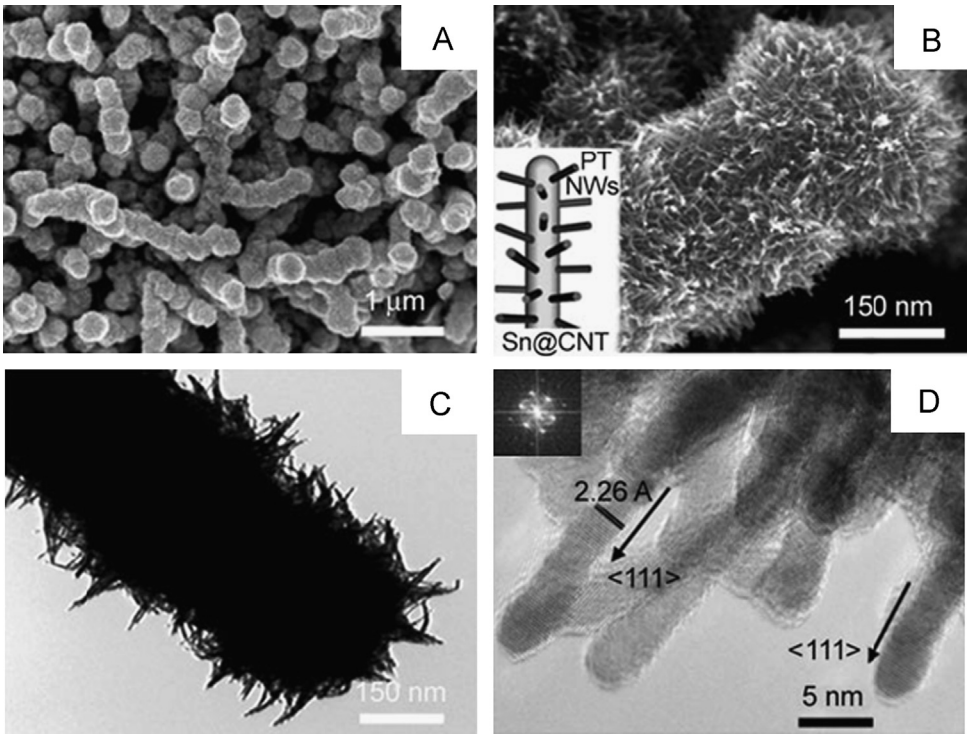

Figure. 9 (A, B) SEM and corresponding HRSEM images of Pt nanowire-Sn@CNT. (C, D) TEM and corresponding HRTEM images of Pt nanowire-Sn@CNT [98]. Reprinted by permission of the Wiley-VCH Verlag GmbH & Co. KGaA.

that PtRuMo in a molar ratio of 6:3:1 had higher catalytic activity and durability for the MOR than homemade PtRu/C and Pt/C. The promotion effect of Mo in the PtRuMo catalyst could be ascribed to the bifunctional mechanism and 'electronic effect' of Mo metal. According to the bifunctional mechanism, MoO_x mixed with Ru further supports H_2O activation, in comparison to Ru alone, which subsequently facilitates CO oxidation, resulting in enhanced MOR activity. Chai et al. [97] prepared Pt-Ru-Co-W quaternary anode electrocatalysts on a conductive substrate by using a robotic dispensing system. According to data analysis, the Pt-Ru-Co-W quaternary anode electrocatalysts exhibited markedly increasing current densities due to the increase in CO_{ads} oxidation by addition of more oxophilic elements to Pt. Sun et al. [98] reported a newly fabricated 3D nanocomposite composed of Pt nanowires and a coaxial nanocable support consisting of a tin nanowire and a CNT (Figure 9). The ultrathin single-crystal Pt nanowire/Sn@CNT was synthesized via a facile surfactant-free aqueous solution method. This 3D Pt nanowire/Sn@CNT electrode exhibited higher MOR activity and improved CO tolerance due to its higher gas permeability, improved metal-support interactions, and enhanced mass transport. Sun et al. [99] synthesized Pt-Ru/CeO_2/MWNT catalysts by a sonication deposition process. They reported a higher electrochemically active surface area of Pt—Ru/CeO_2/MWNT because of a synergistic effect between Pt and the ionic conductor CeO_2, which may promote the hydrogen spillover rate of Pt—H and thus increase the dissociation of hydrogen adsorption.

In addition, Pt—Ru/CeO_2/MWNT displayed the highest oxidative current, further indicating its superior electrochemical performance for the MOR compared to Pt—Ru/MWNT and Pt/MWNT catalysts. This enhancement can be attributed to the bifunctional mechanism, in which CeO_2 may promote the dissociation of coordinated water in the manner of Ru, forming more OH species to oxidize CO_{ad} and release more Pt active sites. Yamazaki et al. developed a CO-tolerant anode catalyst composed of PtRu and a Rh porphyrin [100]. By using this catalyst, hydrogen in the anode gas was oxidized by PtRu, and CO in the anode gas was oxidized via the Rh porphyrin. This porphyrin reduces the CO concentration around Pt—Ru through the CO oxidation process. Kim et al. fabricated shape- and composition-controlled Pt-Fe-Co nanoparticles (nanocubes, branched nanocubes, nanoparticles with low cobalt content and nanoparticles with high cobalt content) for enhanced MOR activity [101]. Pt-Fe-Co branched nanocubes showed the highest activity and durability toward MOR. This substantial increase in MOR activity and durability is attributed to the presence of a small amount of Co, which may have affected the electronic structure of the nanoparticles. Ahn et al. [102] prepared a CoPtRu catalyst through electrochemical methods on a carbon paper substrate. In a typical synthesis of CoPtRu, Co particles were first deposited on carbon paper via an electrodeposition method by changing the deposition potential and time. Subsequently, Pt and Ru galvanic displacements were carried out by controlling displacement time. Compared with other methods, electrochemical processes have many advantages, such as high deposit purity, short preparation time, and facile control of size and composition of the CoPtRu catalyst. Ahn et al. found that the CoPtRu catalysts showed superior catalytic activity for the MOR and better CO tolerance than a commercial PtRu/C catalyst. Sarkar et al. [103] fabricated carbon-supported PtPdCo nanoalloy electrocatalysts by a microwave-assisted solvothermal method. These materials were synthesized at 300 °C without any post-annealing in reducing gas atmospheres. The PtPdCo nanoalloy electrocatalysts showed high tolerance to methanol due to surface strain effects, which developed on the outermost Pt and Pd atomic layers. Saida et al. reported the use of TiO_2 nanosheets (TiO_2ns, $[Ti_4O_9]^{2-}$) as an additive to a PtRu/C anode catalyst for the MOR [104]. The thickness of two-dimensional nanocrystallite TiO_2ns was approximately 1 nm. When TiO_2ns content was low, the mixed TiO_2ns—PtRu/C nanocomposite exhibited high activity and durability due to an increase in the interphase between the electrolyte and PtRu nanoparticles and high ECSA. However, a high content of TiO_2ns tended to have poor current efficiency compared with pristine PtRu/C. Jeon et al. reported a new and economic method to improve the MOR activity of the PtRu catalyst, which was accomplished by mixing the PtRu catalyst with Fe_2O_3 nanoclusters [105]. These authors found that the composite catalyst was more active if 10 wt% Fe_2O_3 was mixed with the PtRu catalyst. The MOR activity was increased by 80% over that of the pure PtRu catalyst. The enhanced MOR activity was attributed to the change in electronic state of Pt through the Fe_2O_3 nanoclusters. Eguiluz et al. [106] synthesized carbon-supported $Pt_x—(RuO_2—M)_{1-x}$ composite ternary catalysts (M=CeO_2, MoO_3, or PbO_x) by the sol-gel process. Carbon-supported $Pt_x—(RuO_2—M)_{1-x}$ composite ternary catalysts were then used as catalysts for the MOR studies. The current density of carbon-supported $Pt_{0.50}(RuO_2—CeO_2)_{0.50}$ catalysts was much higher than that of commercial Pt/C at 450 mV. Due to the oxygen capture and release capacity of ceria, the carbon-supported $Pt_{0.50}(RuO_2—CeO_2)_{0.50}$ catalysts exhibited the highest electrocatalytic activity toward the MOR (onset potential ~207 mV). Li et al. synthesized a tri-component hybrid, such as Pt nanoparticle-polyoxometalate-CNT, via a green approach at room temperature [107]. The polyoxometalates act as both reducing and bridging molecules. The nanohybrid exhibited higher MOR activity than a traditional Pt-C catalyst and other reported Pt/CNT systems due to the following three major factors: (i) the high-conductivity of CNTs facilitated rapid electron transfer between the target molecule and electrode, (ii) the small size of the Pt nanoparticles was beneficial to MOR activities, and (iii) the existence of the layer of polyoxometalate around Pt nanoparticles may be helpful for the catalytic activities and anti-CO-poisoning properties of the catalyst. More recently, Wu et al. fabricated FePt-Au heterostructured nanocrystals (HNCs), such as tadpole-, dumbbell-, bead-, and necklace-like nanostructures by heteroepitaxial growth of Au nanocrystals (NCs) onto FePt nanorods (NRs) [108]. The tadpole-like FePt/C exhibited significantly higher MOR catalytic activity than that of commercial Pt catalysts; this activity was also significantly higher than that of FePt/C catalysts (Figure 10).

Pan et al. [109] fabricated Pt-Sb-doped tin oxide nanoparticles on carbon black (Pt-ATO/C) by using an in situ co-precipitation method and polyol process. The Pt-ATO/C catalyst showed higher MOR activity than the Pt-SnO_2/C or commercial Pt/C catalysts. The enhanced MOR activity

was attributed to the superior electrical conductivity of Sb-doped SnO_2, which induced the electronic effects with Pt catalysts. Liu et al. [110] prepared nanoporous Pt-based multimetallic alloy nanowires by using a template-assisted electrodeposition process. The TEM images and electron diffraction patterns of nanoporous ternary PtCoNi and PtCoAu, as well as quaternary PtRuCoNi nanowires, are shown in Figure 11. As shown in Figure 11, the nanowires were continuous and dense, with uniform diameters along the entire length of the wires. The average diameters for PtCoNi, PtCoAu and PtRuCoNi nanowires were 50, 48 and 45 nm, respectively. Electrochemical measurements indicated that nanoporous $Pt_{57}Co_{31}Ni_{12}$ and $Pt1_8Ru_{15}Co_{48}Ni_{19}$ nanowires markedly enhanced their durability upon continuous potential cycling.

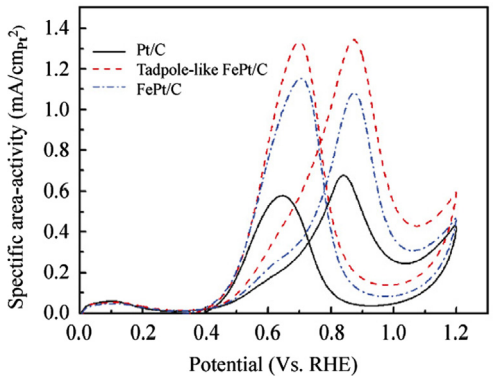

Figure 10 CV curves of the MOR on different catalysts in a 0.5 M HClO4–0.5 M CH_3OH solution [108]. Reprinted by permission of the Tsinghua University Press and Springer-Verlag Berlin Heidelberg.

We have shown experimentally that MOR activity and stability could be enhanced through multiple-component catalysts. However, the present design of multiple-component catalysts may not be optimal because researchers have explored only a limited number of such catalysts. In addition, although these multiple-component catalysts exhibited excellent performance toward the MOR, they still contained high Pt content of more than 50%. Therefore, further research and studies are required to investigate approaches for designing multiple-component catalysts.

New catalyst supports

Multiple-component catalysts are restricted by their low MOR activity, which is due to their low surface area. Because low surface area may restrict widespread use, researchers seek to increase the surface area and improve electrocatalytic activity and utilization. One approach to this problem is use of high surface area materials instead of multiple-component catalysts. The cost of Pt is also an issue of concern. For instance, in 2008, it was estimated that, on the basis of a recent peak price of Pt of over $2200/oz, the cost of Pt alone used in a 100-kW PEMFC engine (~0.8 g/kW) is substantially greater than the current price of an entire internal combustion gasoline engine of equal power [111]. In the last several years, many high surface area based materials have been proposed as Pt supports for DMFCs [112–116]. Regarding this issue, Li et al. [107] synthesized Pt nanoparticle-decorated carbon nanotubes (CNTs) via a green chemistry approach in the presence of polyoxometalates (POMs). The POMs functioned as reducing and bridging molecules in nanohybrids. In addition, due to the superior catalytic properties of POMs, the metal nanoparticles-POM

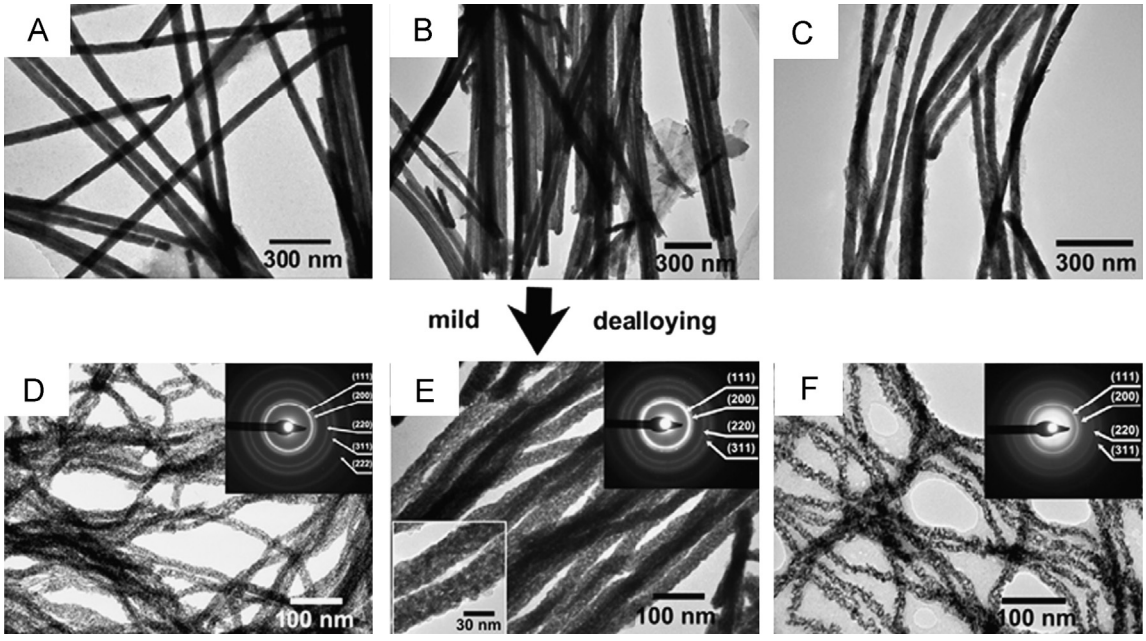

Figure 11 TEM images of the as-prepared nanowires (A) $Pt_1Co_{74}Ni_{25}$, (B) $Pt_4Co_{94}Au_2$ and (C) $Pt_{0.6}Ru_{0.9}Co_{76.4}Ni_{22.1}$, and the dealloyed nanoporous (D) $Pt_{57}Co_{31}Ni_{12}$, (E) $Pt_{30}Co_{56}Au_{14}$, and (F) $Pt_{18}Ru_{15}Co_{48}Ni_{19}$. Electron diffraction patterns of nanowires showed a single set of fcc-like rings (insets of (D)–(F)), suggesting that all nanowires consisted of a single-phase alloy [110]. Reprinted by permission of IOP Publishing Ltd.

composite supported on CNTs may provide enhanced catalytic activities [50]. According to their data analysis, the Pt nanoparticles-POM/CNT exhibited higher electrocatalytic activity towards the MOR than the traditional Pt-C catalyst and other reported Pt/CNT systems. The excellent electrocatalytic performance of the Pt nanoparticles-POM/CNT electrode can be explained as follows. First, the high conductivity of CNTs accelerated electron transfer between the target molecule and electrode. Second, the well-defined small Pt nanoparticles have *enhanced* electrocatalytic activities. Third, the existence of the layer of POM around Pt nanoparticles may be helpful for the electrocatalytic activity and anti-poisoning properties of the catalyst. Hsieh et al. [119] also assembled bimetallic Pt-M (M=Fe, Co, and Ni) on CNT via a two-step chemical reflux method. The CNTs were prepared by catalytic chemical vapor deposition using ethylene and Ni particles as the carbon precursor and catalyst, respectively. On the basis of the electrochemical measurements, the authors found that Pt-Co/CNT catalyst had superior electrochemical activity, anti-poisoning ability, and long-term cycleability relative to Pt-Fe/CNT and Pt-Ni/CNT catalysts due to the bifunctional mechanism of bimetallic catalysts. They reported that two types of mechanisms were involved in enhancing CO tolerance. First, CO adsorption should occur mainly on Pt, while OH should interact preferentially with Co. Thus, the proximity of CO and OH-adsorbed species could explain the promoter effect of Co toward CO oxidation on Pt-Co anode catalysts, leading to a high level of CO tolerance in methanol oxidation. Second, the presence of Co could promote the combined effects of H_2O dissociation and CO oxidation, creating a larger number of active sites for methanol oxidation. Ding et al. [120] synthesized a highly efficient porous hollow carbon nanostructure supporting PtRu catalysts by a one-step pyrolysis process. The PtRu (with 18.5 wt% Pt and atomic ratio of Pt/Ru=1:1) catalysts supported on hollow carbon nanospheres (HCNS) exhibited high electrochemical activity and stability toward the MOR. This enhancement of the MOR catalytic abilities can be attributed to the unique structure of the carbon nanostructure and the pyrolysis-induced high stability and alloying degree of the loaded metallic catalysts. In addition, the PtRu/HCNS catalysts also displayed higher CO tolerance due to the high alloying degree-enhanced bifunctional mechanism, in which Ru supplies an oxygenated surface species by dissociating H_2O at lower potentials with respect to bulk Pt or separated Pt sites. Our groups synthesized a low cost 3D nanoporous graphitic carbon (g-C) material by using an adamantane ($C_{10}H_{16}$) flame [121]. The synthesized g-C was used as a Pt-Ru catalyst support because of its very high surface area. The electrochemical measurements showed that the supported Pt-Ru has higher activity towards the MOR, which is attributed to the presence of 3D nanopores in the g-C support by virtue of which easy transport of methanol and the oxidation products is possible. Joo et al. [122] synthesized highly crystalline graphitic nanocarbons (GNC) by the wet air treatment of hydrothermally derived graphitic porous carbon. They reported that the morphology and degree of graphitic crystallinity changed with temperature. For instance, GNCs consisted of aggregates of silkworm-shaped carbon nanoparticles with enhanced graphitic characteristics at 450 °C. GNC was tested as a Pt catalyst support in the MOR. Based on their results, the Pt/GNC catalyst had a higher electrochemically active surface area than the Pt/C catalyst. These composite catalysts have a positive effect on Pt dispersion, crystallographic orientation, electrical conductivity and electrochemical stability, resulting in the high MOR activity. Sharma et al. [123] prepared reduced graphene oxide/Pt supported electrocatalysts (Pt/RGO) by a microwave-assisted polyol process. The resulting products Pt/RGO exhibited excellent catalytic activity for MOR. They have also found that the CO oxidation activity of the Pt/RGO hybrid electrode was higher than that of the commercial Pt/C catalysts due to the presence of residual oxygen groups on RGO.

Three possible mechanisms were involved in enhancing the CO tolerance and methanol oxidation of these materials.

First, RGO promotes water activation due to its hydrophilic nature. Thus, the adsorbed OH species at the Pt edge promote CO oxidation.

Second, strong interaction between Pt and RGO was found, which can induce some modulation in the electronic structure of Pt clusters, modifying the Pt—CO binding energy and, as a result, minimizing CO adsorption on Pt.

Third, Pt/RGO catalysts can promote hydrogen spillover (the process involving dissociative chemisorption of molecular hydrogen on a supported Pt catalyst surface, followed by the diffusion of atomic hydrogen onto the surface of RGO). The RGO species on the Pt surface promote the formation of —GO) species adjacent to CO-poisoned Pt sites, which combine with adsorbed CO to strip it from the surface as CO_2.

Pt/TiC was prepared by using a simple electrodeposition process to load Pt nanoparticles on TiC nanocomposite by Ou et al. [124]. They reported that the Pt/TiC catalyst is able to reduce the risk of the CO poisoning effect for the MOR. The enhancement in the MOR catalytic activity was ascribed to OH groups (formed by water discharge on the TiC surface) promoting CO removal near the Pt-oxide interface and strong metal support interaction. Tiwari et al. [125] prepared amorphous carbon-coated silicon nanocones (SiNCs) by an anodic aluminum oxide (AAO) templation method and microwave plasma chemical vapor deposition (MPCVD). The Pt nanoparticles were electrodeposited on amorphous carbon-coated SiNCs (Pt/ACNC) and used as the catalyst for the MOR. The Pt/ACNC catalyst showed superior MOR performance in terms of mass activity and current density. The higher MOR activity of the Pt/ACNC catalyst could be attributed to the large ECSA. In addition, the small (nm scale) Pt catalyst nanoparticles could increase CO oxidation via the bi-functional and L-H mechanisms, producing more active Pt sites for the MOR and thus enhancing MOR efficiency. To further enhance MOR activity, Tiwari et al. synthesized 3D Pt nanopetals on SiNCs by pulse-electrodeposition [126]. A CV study on the 3D Pt nanopetals/SiNCs electrode revealed higher current density than those of Pt nanoparticles/flat Si and Pt nanoflowers/flat Si electrodes. The higher MOR activity was attributed to abundance of a large ECSA for facile transport of methanol, SiO_2 sites in the vicinity of the SiNCs, as well as less contact area between the Pt nanopetal catalyst and SiNCs. Fang et al. [127] synthesized Pt nanoparticles with an average size of 3.14 nm on N-doped CNTs by a chemical approach.

The Pt/N-doped CNTs exhibited the best catalytic activity because the so-called N incorporation could be used to produce preferential sites of CNTs with low interfacial energy for immobilizing Pt nanoparticles.

More recently, graphene has been studied as a catalyst support in DMFCs due to its basal plane structure with high surface area (calculated value, 2630 m^2/g), high conductivity (10^3—10^4 S/m) and potentially low manufacturing cost [128-131]. Zhou et al. [132] fabricated graphene-supported Pt nanoparticles via a one-step electrochemical approach. According to their data, Pt nanoparticles on graphene exhibited much higher catalytic activity and long-term stability towards the MOR than the Pt nanoparticles on Vulcan. Guo et al. [133] also fabricated high-quality 3D Pt-on-Pd bimetallic nanodendrites/graphene nanosheets by a wet-chemical approach. Due to their high ECSA, the graphene/bimetallic nanodendrite hybrids showed much higher electrocatalytic activity toward the MOR than Pt black and commercial E-TEK Pt/C catalysts. They also reported that the number of branches for Pt-on-Pd bimetallic nanodendrites on graphene nanosheets was controlled by a few experimental parameters, thus resulting in increased catalytic properties. Joo et al. [122] synthesized highly crystalline graphitic nanocarbons (GNC) by the wet-air treatment of hydrothermally (450 °C) derived graphitic porous carbon. At 450 °C, the products consisted of aggregates of silkworm-shaped carbon nanoparticles with enhanced graphitic properties. The Pt nanoparticles were coated on GNC by a reduction method (sodium ethoxide as the reducing agent). Pt/GNC exhibited the highest MOR activity (Figure 12) due to enhanced graphitic characteristics with highly dispersed Pt nanoparticles on the graphitic layers.

Zhang et al. prepared large-scale single-crystalline hollow nanobowls of pure C_{60} by applying a sonophysical strategy in a binary organic solution of m-xylene and acetonitrile [135]. The Pt nanoparticles were deposited by electrolytic reduction of an aqueous solution of $PtCl_6^{2-}$. Figure 13 (A, B) shows the SEM images of the resulting Pt/C_{60} hollow nanobowl. As shown in Figure 13 (A, B) the Pt nanoparticles were deposited well on both the outside and inside surfaces of the C_{60} hollow nanobowls. Due to the high surface area of the Pt/C_{60} hollow nanobowl, these hollow nanobowls exhibited significantly enhanced catalytic activity toward the MOR (at 0.65 V, Figure 13 C).

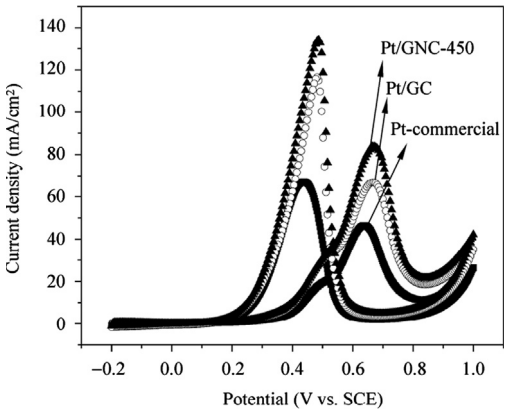

Figure 12 CV curves of the three catalysts were collected in a 0.5 M H_2SO_4–1 M CH_3OH solution. Reprinted by permission of the Tsinghua University Press and Springer-Verlag Berlin Heidelberg.

A quick literature survey can easily give readers many articles on support materials with highly active surface areas, such as 2D or 3D nanostructures, for good dispersion of catalysts [136,137]. Oh et al. [137] fabricated a 3D TiO_2 nanostructure support by a seeding process with 1D TiO_2 nanowires as a seed. The Pt/3D TiO_2 catalysts exhibited much-enhanced catalytic activity and stability toward the MOR due to its high specific surface area and improved electronic transfer efficiency via 3D TiO_2 nanostructure support.

Only a few supported materials (CNT, GNC, g-C, RGO, SiNC, TiC, TiO_2) have been invented for anode catalysts, which is more crucial in enhancing DMFC performance. Therefore, materials scientists must find a newer and better supported material that converts a fuel source directly into electrical energy.

Cathode catalysts of DMFCs

Like the anode electrode, the cathode electrode of DMFCs also lacks an adequate electrocatalyst. Therefore, it is necessary to develop new cathode electrocatalysts (low cost and better durability) that have high electrocatalytic activity for the oxygen reduction reaction at low temperatures. In the following section, recent progress in the development of cathode electrocatalysts for DMFCs is discussed in detail. For a detailed discussion of cathode electrocatalysts, we collected more than 100 recently published works from different journals.

Single-component catalysts

As a common catalyst for the ORR, noble metals contribute significantly to DMFCs [138-145]. However, there are still some problems, such as sluggish kinetics and poor electrocatalyst durability of the ORR at the cathode, that limit the efficiency of DMFCs. Therefore, development of a highly active and durable catalyst is greatly sought to improve the ORR performance of DMFCs. The goal for materials scientists is to find various kinds of catalysts to enhance the activity for the ORR. In this regard, researchers began their search with single-component catalysts. In the past decade, several single-component catalysts were reported by materials scientists. There have been several single-component catalysts (such as Ag [138], Au [138,139], Pt [140], Pd [141,142], nitrogen (N)-doped graphitic carbon [135], N-based carbon nitride [144], MoN [145], N-doped carbon nanotubes (CNTs) [146]) that have shown improvements of ORR activity. In addition, carbon materials have been identified as some of the most promising materials for DMFCs in acidic media due to their high chemical stabilities, high electric conductivities and enhanced mass transport capabilities [147]. Modifying carbon materials by different N-functional groups is known to enhance their activities for the ORR [148]. Various types of N-functional groups can be initiated on carbon surfaces by varying the experimental procedure and parameters [149]. N-doped carbon materials

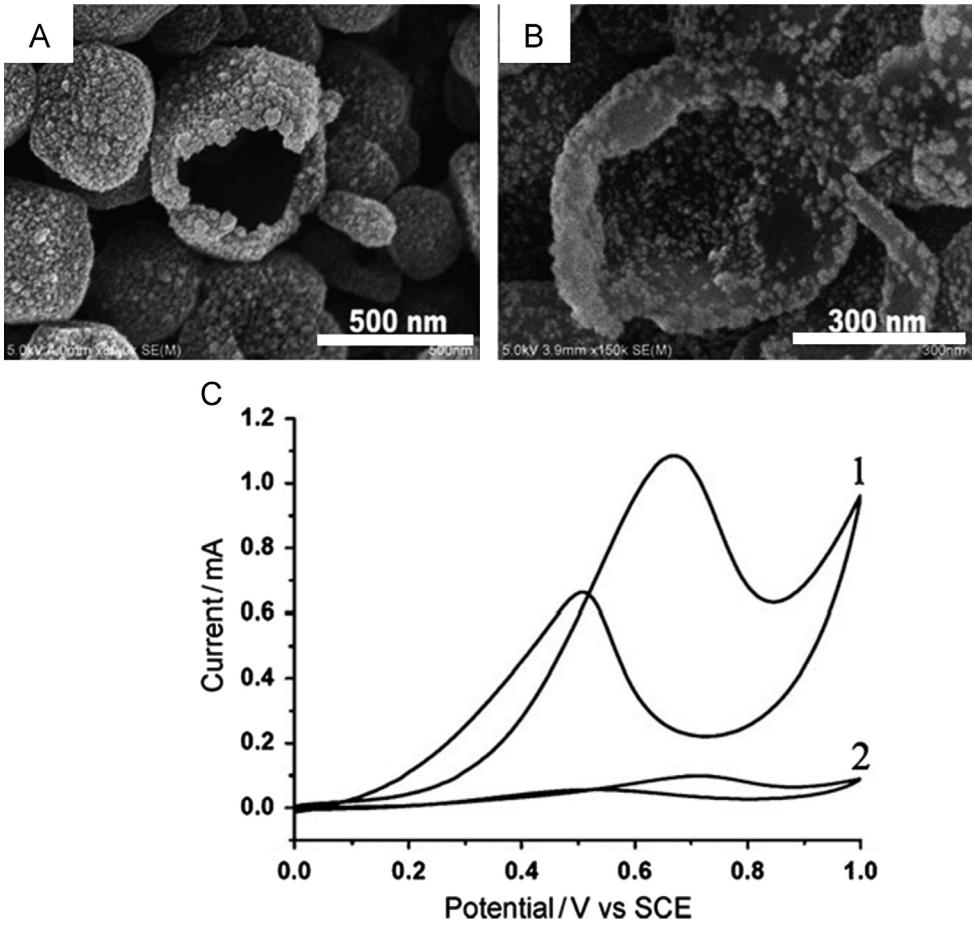

Figure 13 SEM images of Pt-deposited C_{60} hollow nanobowls (A) outside Pt deposition and (B) inside Pt deposition. (C) CV curves of (1) Pt/C_{60} hollow nanobowl and (2) Pt/C_{60} solid nanoball (2) electrodes in a 0.1 M H_2SO_4–2 M CH_3OH solution [135]. Reprinted by permission of the Wiley-VCH Verlag GmbH & Co. KGaA.

have pyridinic and pyridinic-N-oxides as nitrogen species, which are responsible for the enhanced ORR activity [150]. N-functional groups transform to more thermally stable structures during heat treatment [149]. Furthermore, nitrogen is also known to efficiently create defects on carbon materials, which may increase the edge plane exposure and thus enhance the ORR activity [151]. Nagaiah et al. [146] synthesized N-doped CNTs (NCNTs) by treating HNO_3-oxidized CNTs (OCNTs) in ammonia flow (25 sccm) at 200 °C (NCNT-200), 400 °C (NCNT-400), 600 °C (NCNT-600) and 800 °C (NCNT-800) for 6 h. They found that NCNT-800 showed greatly enhanced ORR activity in alkaline media. In addition, NCNT-800 also showed a favorable positive onset potential for the ORR, increased reduction currents, and high stability. Liu et al. [143] fabricated N-doped ordered mesoporous graphitic arrays (NOMGAs) on the basis of a metal-free casting technology. Mesoporous silica (SBA-15) and N, N′-bis(2,6-diisopropyphenyl)- 3,4,9,10-perylene-tetracarboxylic diimide (PDI) were used as the template and carbon precursor, respectively. NOMGAs with different compositions were fabricated by the carbonization of PDI/SBA-15 composites at 600, 750, and 900 °C; the resulting materials are represented as PDI-600, PDI-750, and PDI-900, respectively. The ORR activities of Pt-C, PDI-600, PDI-750, and PDI-900 catalysts are shown in Figure 14. As shown in Figure 14, PDI-900 catalysts showed greater ORR activity than did PDI-600, PDI-750, and commercially available Pt-C catalysts. According to this report, the electron transferred value of PDI-900 is ~3.89. The results have shown that the PDI-900 catalyst acts as a 4-electron transfer for the ORR. The unique features of the PDI-900 catalyst, including high surface area and a graphitic framework with a moderate N content, led to high ORR activity, excellent stability, and resistance to crossover effects for the ORR. More recently, Yang et al. [144] fabricated graphene-based carbon nitride (G-CN) nanosheets and studied their ORR properties. They found that the G-CN nanosheets not only possess high N contents, low thicknesses, high surface areas, and large aspect ratios but also show enhanced electrical conductivity. The above properties are favorable for the access of O_2 to the catalyst surface and can facilitate the fast diffusion of electrons in the electrode during the ORR process. As a result, the G-CN nanosheets exhibited excellent ORR activity, high electrocatalytic activity, long-term durability, and high selectivity, compared to those of CN sheets and Pt-C catalysts (Figure 14).

Although metal-free catalysts such as G-CN nanosheets, PDI-900 catalysts and NCNT-800 have low costs, the commercial viability of DMFCs is still hindered by poor kinetics and slow ORR activity.

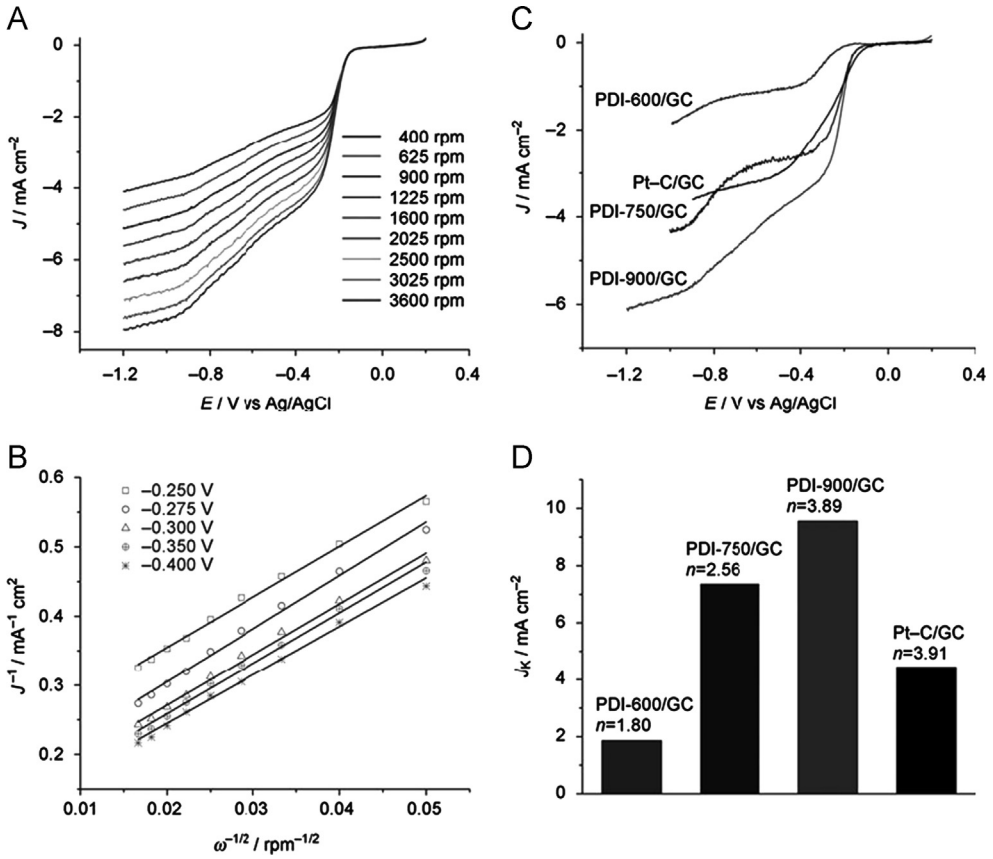

Figure 14 (A) CV curves of G-CN800 in O_2-saturated 0.1 M KOH with different rotation speeds at a constant scan rate of 5 mV s^{-1}. (B) Koutecky-Levich plots of G-CN800 obtained from CV curves in (A) at various electrode potentials. (C) CV curves of G-CN and CN nanosheets at a constant rotation rate of 1600 rpm. (D) Electrochemical activity, shown as the kinetic-limiting current density (J_K) at −0.40 V [143]. Reprinted by permission of the Wiley-VCH Verlag GmbH & Co. KGaA.

The search for a stable and more active electrocatalyst for ORR activity in acidic and alkaline media is thus of great importance. As a consequence, the development of single-component (such as Pt, Ag, Pd or Au) catalysts with high ORR activity has recently become a major focus of DMFC research. Kuai et al. [138] reported uniform, high-yield (>90%) icosahedral Ag and Au nanoparticles by using a hydrothermal system in the presence of PVP and ammonia. The Ag and Au icosahedra showed excellent stability and much higher electrocatalytic activity than spherical nanoparticles; they exhibit positive shifts in the reduction peak potential for oxygen of 0.14 and 0.05 V, while the reduction peak currents of the Ag and Au icosahedra were 1.5- and 1.6-fold, respectively, better than those of spherical nanoparticles and Pt/C catalysts. Jeyabharathi et al. [139] electrodeposited Au atomic clusters in the presence of cetyltrimethylammonium bromide (CTAB) and studied their ORR catalytic activities. Some interesting properties were exhibited by such clusters: (a) molecule-like voltammetric features; (b) electrocatalysis of the oxygen reduction to H_2O via a 4-electron pathway in acidic media; and (C) representation of a transition of the ORR mechanism from four-electron to two-electron reduction [139]. At present, the most widely used cathode catalyst consists of Pt nanoparticles due to its high ORR activity. Therefore, many researchers synthesized metal-based nanostructured materials for kinetically enhancing the sluggish electrode reaction [138,139,142,152]. Wang et al. [153] reported a simple method to monodisperse Pt nanoparticles with a nanometer size range (3–7 nm) and controlled polyhedral, truncated cubic, or cubic shapes; they also studied their ORR activities. In their synthesis, the sizes and shapes of the Pt nanoparticles were controlled by the reaction temperature. Figure 15 displays TEM images of the 3, 5, and 7 nm Pt nanoparticles.

The inset of each TEM image shows a high-resolution TEM image of a single nanoparticle. The inset of Figure 15 (A) corresponds to Pt (111) lattice fringe. However, the insets of Figure 15 (B, C) correspond to Pt(100) and Pt(100) lattice fringes. According to their data, Wang et al. found that the current density from the ORR for Pt nanocubes is 4-fold that of polyhedral Pt or truncated cubic Pt nanoparticles, showing that ORR activity is indeed dependent on the shape, not on the size, of the Pt nanoparticles. More recently, Yu et al. [154] fabricated Pt concave nanocubes enclosed by high-index facets, including (510), (720), and (830), via addition of a $NaBH_4$ solution and a mixture containing K_2PtCl_4, KBr, and $Na_2H_2P_2O_7$ into DI water. In a typical synthesis, the pyrophosphato complex and the slow addition of this precursor by a syringe pump contributed to the formation of Pt concave nanocubes. In this regard, the seeds selectively overgrow from corners and edges, and the Br^- ion acts as a capping agent to block the (100) facets. The Pt concave nanocubes showed substantially enhanced ORR activity relative to that of Pt nanocubes, cuboctahedra, and commercial Pt/C catalysts that are bounded by

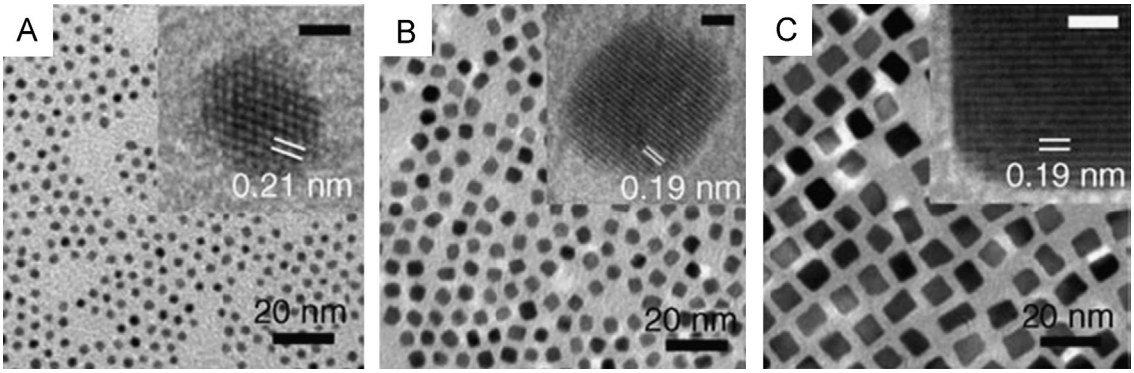

Figure 15 TEM and HRTEM images of (A) 3 nm, (B) 5 nm, and (C) 7 nm Pt nanoparticles [153]. Reprinted by permission of the Wiley-VCH Verlag GmbH & Co. KGaA.

low-index facets such as (100) and (111). Further, ORR activity can be enhanced through free-standing Pt-nanowires because these nanowires possess many novel structural characteristics, including flexibility, large area per unit volume, high stability, preferential exposure of highly active crystal facets, and easy electron transport [155–157]. To address this issue, Liang et al. [158] used a templating method to prepare a free-standing Pt nanowire, and its ORR activity was studied. The free-standing Pt nanowire catalyst exhibited high stability compared with Pt/C and Pt black. The free-standing Pt catalyst exhibited remarkably high stability because of its unique supportless nanowire network structure (rapid electron transport and gas diffusion) and the preferential exposure of certain crystal facets in 1D Pt nanowires. Wang et al. [159] synthesized a Pt nanoparticle netlike assembly through a hydrothermal method. The Pt nanoparticle netlike assembly exhibited higher durability and 2.9 times higher mass activity for ORR than the commercial Pt black catalyst due to its high specific surface area and large overall size. Porous nanotubes exhibited several novel structural characteristics, including high porosity, flexibility, large area per unit volume, and an interconnected open pore structure. Alia et al. [39] fabricated porous Pt nanotubes with a thickness of 5 nm, an outer diameter of 60 nm, and a length of 5–20 μm. The porous Pt nanotubes were synthesized by galvanic displacement with Ag nanowires, which were obtained by the ethylene glycol reduction of silver nitrate. They also evaluated the ORR activity and durability of porous Pt nanotubes, and they found that the stability and ORR activity of porous Pt nanotubes are much higher than those of Pt/C and bulk polycrystalline Pt catalysts. Although single component metals (such as Pt, Pd or Au) have high ORR activity and stability, dissolution/agglomeration of these single-component metals from cathodic catalysts contribute to the performance decay of DMFCs. Furthermore, researchers believe that the stability and activity of the Pt-based fibrous membrane catalyst can be further improved by alloying with other metals to form binary catalysts.

Double-component catalysts

As we discussed above, single-component nanostructured catalysts such as Pt, Pd, and Au can increase ORR activity relative to Pt, Pd, and Au bulk metals [161]. Among these catalysts, nanostructured Pt is a traditionally great electrocatalyst for ORR but is very costly for commercialization in DMFCs [162]. To utilize Pt loading in a limited resource, double-component nanostructures are developed. In 2005, Wang et al. [163] showed that ORR activity would be enhanced by coupling a metal X (X=Co, Ni, Cr, or V) with a low occupancy of *d*-orbitals with another metal X′ (such as X′=Pd, Ag, and Au) with fully occupied *d*-orbitals [154]. The *d*-orbital coupling effect between metals can significantly decrease the Gibbs free energy for the electron transfer steps in the ORR, resulting in enhanced ORR kinetics [163]. Xia et al. [145] synthesized a MoN electrocatalyst via heat treatment of molybdenum tetraphenylporphyrin in the presence of a gaseous atmosphere of ammonia. The synthesis was followed by heat treatment at various temperatures in the presence of ammonia gas. In the presence of ammonia, the following type of reaction may occur and provide the source of N for MoN formation:

$$2NH_3 = 3H_2 + 2[N] \quad (10)$$

The electrochemical measurements showed that the MoN catalyst has strong ORR activity, proceeding by an approximate four-electron pathway (the electron transfer number calculated based on the measured slope value was ~3.8, which is very close to 4), through which molecular oxygen is directly reduced to water by accepting four electrons. Sarkar et al. [165] synthesized Pd-W nanoalloy electrocatalysts by simultaneous thermal decomposition of palladium acetylacetonate and tungsten carbonyl in o-xylene in the presence of Vulcan XC-72R carbon, followed by annealing up to 800 °C in a hydrogen environment. Low cost Pd-W nanoalloy is found to increase both the catalytic activity for ORR and the catalyst durability. In addition, Pd-W nanoalloy catalysts offer the important advantage of high tolerance to methanol compared to Pt. The origin of the enhanced ORR activity has been attributed to the following characteristics: (i) modification of the electronic structure of Pt (5*d*-orbital vacancies), (ii) changes in the Pt-Pt bond distance and coordination number, and (iii) inhibition of adsorbed oxygen-containing species from the electrolyte onto Pt. In 2008, Camargo et al. [166] synthesized $RuSe_{2+d}$ nanotubes as an electrocatalyst for the ORR. These nanotubes were synthesized by template-engaged replacement

reactions (TERR). The TERR was able to create hollow nanostructures of novel metals. $RuSe_{2+d}$ nanotubes were obtained by TERR between $Ru(acac)_3$ and *t*-Se nanowires at 80 °C, followed by selective removal of the unreacted *t*-Se cores. $RuSe_{2+d}$ nanotubes were highly active for the ORR and showed high tolerance to 0.1 M CH_3OH. While the mass-specific ORR activities at 0.7 V were ~30 times lower than that of Pt/C catalysts, no detrimental effect on the ORR activity was observed upon the mixing of 0.1 M CH_3OH. In the presence of 0.1 M CH_3OH, the mass-specific ORR activity of $RuSe_{2+\delta}$ was ~12 times lower than that of Pt/C at 0.7 V. In addition to high methanol tolerance, the $RuSe_{2+d}$ catalyst also exhibits high ORR stability relative to Pt/C. In 2009, Liu et al. [167] synthesized a Pd_4Co nanoalloy by a modified polyol process; the polyol process exploits high-boiling polyalcohol solvents as mild reducing agents at moderate temperatures and offers a facile method for producing multi-metallic alloy nanoparticles in the absence of solid state diffusion over large atomic distances. The synthesis of Pd_4Co nanoalloy involved a mixture of ethylene glycol and a small amount of $NaBH_4$ as reducing agents, and the resulting material was evaluated in fuel cells to demonstrate ORR activity and durability. The Pd_4Co nanoalloy annealed at 350 °C exhibited high ORR catalytic activity due to an increase in the degree of alloying. Remona et al. [168] synthesized Pt-Bi on carbon (Pt_3Bi/C, PtBi/C and $PtBi_3/C$) by reducing the aqueous metal ions using $NaBH_4$ in the presence of a microemulsion. The Pt_3Bi/C, PtBi/C and $PtBi_3/C$ catalysts displayed higher methanol tolerance for ORR than Pt/C of the same metal loading. In addition to high CH_3OH tolerance, all Pt-Bi/C catalysts exhibited higher mass activities for the ORR (1-1.5 times) than Pt/C. The high ORR activity of all Pt-Bi/C catalysts was found to be due to the distortion (internal stress) of three Pt site requirements by bismuth (third-body effect). In 2010, Lai et al. [169] reported the dealloying mechanism for Pt-Co bimetallic alloys and investigated the catalytic activity of the ORR via cyclic voltammograms (CVs). Figure 16 shows typical CVs for the ORR at different chemical dealloying times in O_2-saturated 0.5 M H_2SO_4. The ORR was diffusion-controlled when the potential was less than or equal to 0.7 V but was under mixed diffusion-kinetic control in the potential region between 0.7 and 0.85 V. Potentials greater than 0.85 V resulted in kinetic control. The Pt-Co nanoparticles exhibited better ORR catalytic performance after 2 h of chemical dealloying and a positive shift of ~17.3 mV in the half-wave potential relative to the initial step. However, after 4 h of chemical dealloying, the CVs and ORR activity reveal an inferior function of the catalyst. A Pt-rich core with Co-rich shell structures is likely formed in Pt-Co nanoparticles. As dealloying proceeds, the Co-Co bond dissolves gradually and results in smaller nanoparticles with rough, imperfect Pt skin with sculpted shapes. As shown in Figure 16, Pt-Co nanoparticles have better catalytic performance for the ORR after dealloying for 2 h. However, after 4 h of chemical dealloying, the electrolyte penetrating into the imperfect Pt skin dissolves cobalt present in the underlying layers, and the surface features of the nanoparticles finally collapse.

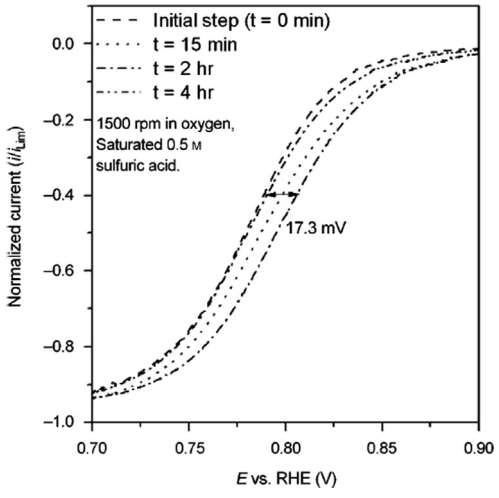

Figure 16 Steady-state CVs for the ORR obtained at 1 m Vs^{-1} at different chemical dealloying times [159]. Reprinted by permission of the Wiley-VCH Verlag GmbH & Co. KGaA.

A systematic investigation of the structural and electronic effects of Pt_xPd_{1-x} bimetallic nanoparticles on the ORR in acidic media was performed by Chang et al. [170]. They synthesized Pt_xPd_{1-x} nanocatalysts with different Pt:Pd atomic ratios (x=0.25, 0.5, and 0.75) by using a borohydride-reduction process. ORR activity can be enhanced through the high number of alloying and low Pt d-band vacancies, owing to favorable O-O scission and inhibited formation of oxygenated intermediates. They also reported that ORR reactivity depends on the composition of alloying and d-band vacancies of the Pt_xPd_{1-x} nanocatalysts such that there was a synergistic effect on ORR activity. Li et al. [171] synthesized Pt-Fe bimetallic nanocatalysts (Pt-Fe/C) with different Pt:Fe ratios by a modified ethylene glycol (EG) method and then heat treated in the presence of H_2-Ar gas at 900 °C. The Pt-Fe (Pt:Fe ratio of 1.2) electrode showed higher DMFC performance at 90 °C than Pt/C and Pt-Fe (different atomic ratio) catalysts, which is attributed to its smaller nanoparticle size and improved Pt-Fe alloy structure. Among the various double-component catalysts, the most promising double-component cathode materials developed to date for DMFCs are Pt-Au bimetallic catalysts. The Pt-Au catalyst showed very high ORR catalytic activity and stability [172,173]. In 2010, Xu et al. [174] prepared a series of carbon supported Pt-Au nanoparticles by the dimethylformamide co-reduction process. From ORR results, they summarized that a 30PtAu14/C (Pt loading: 30 wt%) sample exhibited poor ORR activity in acidic electrolytes, compared to 30Pt/C and 30PtAu13/C. In addition, the onset potential of the 30Pt/C catalyst in O_2-saturated electrolytes becomes much higher than that of the 30PtAu14/C and 30PtAu13/C catalysts. This result suggests that unfavorable O_2 adsorption on the surface of the catalyst, mainly due to the addition of Au atoms, decreases the number of active sites for O_2 adsorption. In the same year, Kim et al. [175] synthesized heterogeneous bimetallic nanocrystals consisting of Pt multibranches on Au nanocrystal cores with well-defined morphologies (cubes, rods, and octahedra), as shown in Figure 17.

AuPt bimetallic heteronanostructures were used to study their catalytic activity for the ORR. The results suggest that AuPt bimetallic nanostructures display higher catalytic activity and durability for the ORR than the monometallic

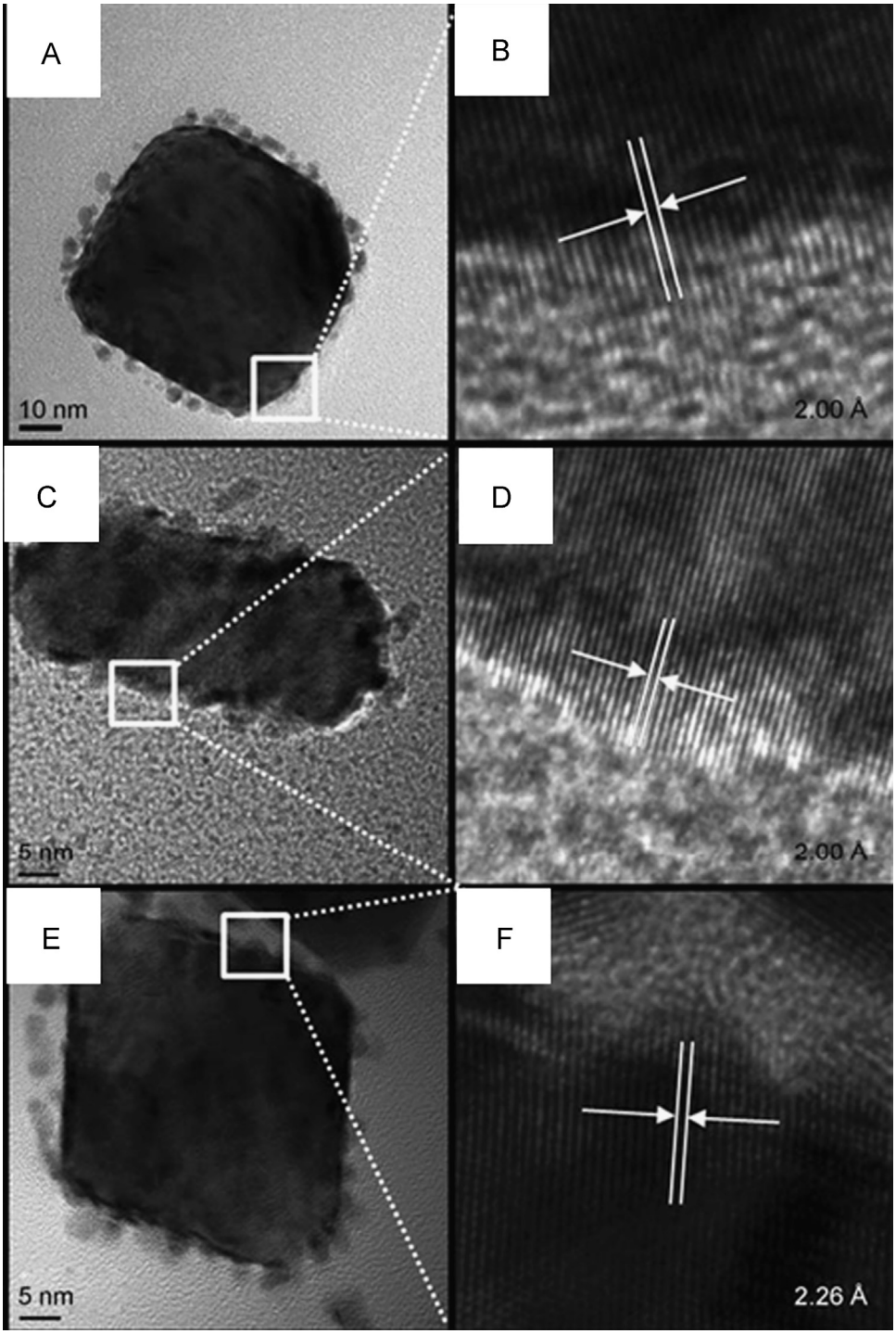

Figure 17 HRTEM images with low- and high-magnification of Au_{cube}@Pt (A,B), Au_{rod}@Pt (C,D), and $Au_{octahedron}$@Pt (E,F) [175]. Reprinted by permission of the Wiley-VCH Verlag GmbH & Co. KGaA.

Pt catalyst. Thus, the formation of heterostructures can supply more active catalytic surfaces. In addition, it was found that ORR activity is dependent on the shape of the cores. The use of an Au nano-octahedron core resulted in improved enhancement of ORR activity. Dutta et al. [176] prepared a bimetallic Pt—Cu oxygen reduction catalyst by a multistep synthetic procedure. Three steps were involved in the typical synthesis of the Pt—Cu catalyst: (1) reduction of Pt and Cu chloride salts with hydrazine hydrate to yield carbon-supported metal nanoparticles, (2) annealing to produce alloy nanoparticles, and (3) chemical dealloying of the catalyst nanoparticles to produce the "dealloyed catalyst". Due to the increase in surface area, the ORR mass activity of the Pt—Cu catalyst was 3 times higher in terms of Pt-based mass activity. More recently, Yeo et al. [177] prepared a uniform Pt nanodendrite structure via seed-mediated growth

inside hollow silica nanospheres (Figure 18). The seed-mediated growth procedure produced Pt-on-Au nanodendrites in a ligand-free form on a gram scale.

According to data analysis, the Pt-on-Au nanodendrites have shown higher ORR activity than commercial Pt black catalysts. The improvement of ORR activity was due to the presence of a large number of edges and corner atoms, as well as the high catalytically effective surface area. Recently, one-dimensional (1D) nanostructures (compared to the 0D nanostructure of Pt nanoparticles) have been emerging as a new approach to avoid agglomerations, dissolution, Ostwald ripening, and aggregation during fuel cell operation [178,179]. Zhang et al. [179] synthesized ultra-thin Pt_xFe_y-nanowires with diameters of 2–4 nm via a solution-phase reduction method at Pt-Fe compositions from 1:1 to 2:1 (Figure 19). The ultra-thin Pt_xFe_y-nanowires have higher electrochemical surface areas (52 $m^2\ g^{-1}$) and better Pt utilization (76% for Pt_1Fe_1-NW) than Pt/C. In addition, these nanowires displayed higher ORR activity and electrochemical durability. The improved durability may be due to the high aspect ratio 1D nanowire structure and spin-orbit coupling and hybridization between Fe and Pt; the higher ORR activity may arise from electronic effects.

In an effort to explore cost-effective and methanol-tolerant cathode catalysts for DMFCs, non-noble or non-Pt catalysts seem to be favored. In this regard, Fujigaya et al. [180] developed a low-cost Pt-free catalyst as a cathodic electrocatalyst for the ORR. They prepared N-containing core/shell CNTs through wrapping MWCNTs with pyridyl links, followed by Co-coordination and calcination. The N-containing core/shell CNTs exhibited significantly higher ORR activity. The high ORR activity was attributed to the N-containing graphitic structure in the shell.

From the above discussion and examples, it should be clear that double-component catalysts have been found to exhibit high activity for the ORR. However, the dissolution of both transition metals limits their application in DMFCs. The dissolution of double-component catalysts could result in a decrease in catalyst activity for the ORR. The catalyst activity is enhanced by the substitution of components in the double-component catalysts.

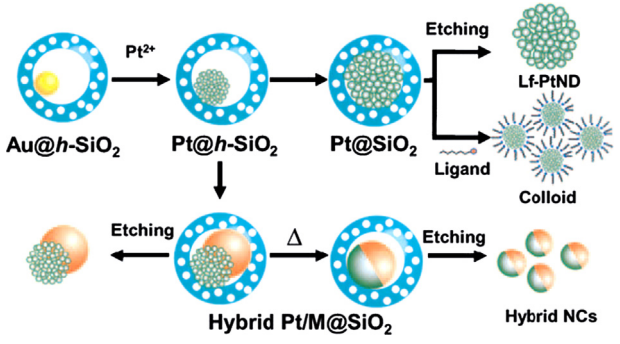

Figure 18 Schematic diagram for synthesis of Pt-based nanodendrites and hybrid nanocrystals [177]. Reprinted by permission of the Wiley-VCH Verlag GmbH & Co. KGaA.

Multiple-Component Catalysts

As stated above, the high cost of electrocatalysts is one of the major obstacles to the commercialization of DMFCs. In addition, double-component catalysts have the problem of metal dissolution. One possible way to overcome the dissolution as well as improve the stability of electrocatalysts is to prepare multiple-component catalysts. By using multiple-component systems, we may shift the *d*-band center by a strain effect (caused by the lattice mismatch in the multiple-component systems), lower the adsorption energy of surface oxygenated intermediates, and thus enhance the surface catalytic activity. Over the years, many efforts have been made to synthesis new catalyst systems for the reduction of oxygen based on multiple-component catalysts such as PtTiM (M=Co, Cr, Cu, Fe, Mn, Mo, Ni, Pd, Ta, V, W and Zr) [181], PtCuCo [182], Pt/$CoSe_2$ nanobelts [183], PdCo@Pd core-shell [184], PdSn/Pt [185], PtIrCo [186], core/shell Pd/FePt [187], Pt/$Ti0_{.7}W_{0.3}O_2$ [188] and Pt nanowires on Sn@CNT [98]. More recently, Liu et al. [190] synthesized low Pt-content quaternary PtCuCoNi nanotubes via a template-assisted electrodeposition process and measurement of the suitability of these hollow multimetallic nanotubes as effective ORR electrocatalysts. The electrochemical active surface area (ECSA) of the PtCuCoNi nanotubes, Pt/C and Pt black are 104.1, 49.8 and 14.7 $m^2\ g_{Pt}^{-1}$, respectively (calculated from Figure 20 (A)). In addition, the half-wave potentials ($E_{1/2}$) of the PtCuCoNi nanotubes, Pt/C and Pt black are 0.87, 0.84 and 0.74 V, respectively (Figure 20 B). Due to their unique combination of micrometer-sized length and hollow configuration, the PtCuCoNi nanotubes had superior ORR performance over both Pt black and Pt/C catalysts.

Zhang et al. [185] synthesized a carbon-supported PdSn@Pt catalyst with a core-shell structure by a two-stage route. In a typical process, a PdSn/C catalyst with a

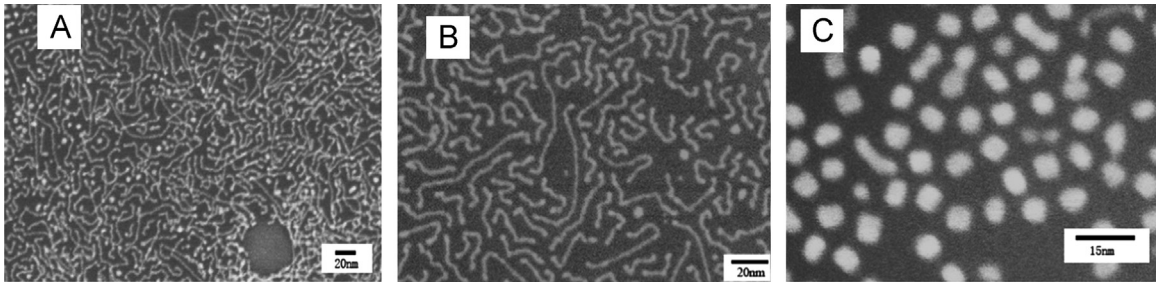

Figure 19 TEM images of Pt-Fe nanowires with different diameters: (A) 2.7 nm, (B) 2.9 nm, and (C) 4.2 nm [179]. Reprinted by permission of IOP Publishing Ltd.

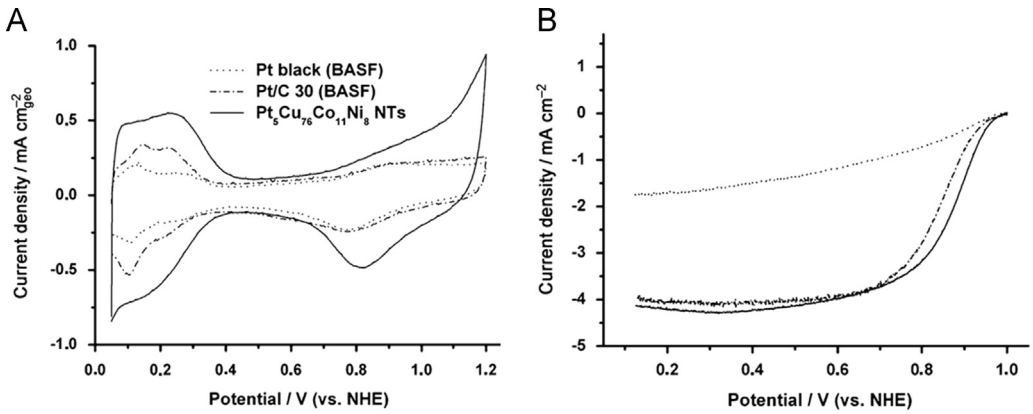

Figure 20 (A) CV curves collected for Ar-saturated 0.1 M $HClO_4$ solution at a scan rate of 50 mV s^{-1}. (B) Polarization curves collected in O_2-saturated 0.1 M $HClO_4$ solution at a scan rate of 10 mV s^{-1} and a rotational rate of 1600 rpm [190]. Reprinted by permission of the Wiley-VCH Verlag GmbH & Co. KGaA.

nominal atomic ratio Pd: Sn = 1:1 was first prepared. The pH value of the PdSn/C mixture was then adjusted to ~9 by the drop-wise addition of a 5 wt% KOH/EG solution. The mixture was then placed into a round-bottom flask, and the temperature was maintained at 160 °C for 8 h; the resultant product was collected by filtration, washed with deionized (DI) water and dried in air. In the second step, appropriate amounts of $H_2PtCl_6 \cdot 6H_2O$ were added to PdSn/C powders, and the mixture was stirred for 4 h at 80 °C. Finally, the powders were collected by filtration and then washed with DI water to remove the chloride anion. Zhang et al. [185] also studied the ORR activity of the PdSn@Pt/C catalyst. They hypothesize the following reasons for the enhanced catalytic activity for the ORR of the PdSn@Pt/C catalyst over the Pt/C catalyst:

(1) PdSn@Pt/C catalyst has a higher surface area, which provides more active sites and results in higher catalytic activity.
(2) The core–shell nanostructure increases the utilization efficiency of precious metal catalysts.
(3) The electronic effect between PdSn alloy and Pt.

Yang et al. [191] synthesized a carbon-supported PdCo@PdPt/C catalyst via a simple galvanic replacement reaction. They also found that the PdCo@PdPt/C catalyst had very high activity towards the ORR in acidic solutions both with and without methanol. The PdCo@PdPt/C catalyst showed 4–6-fold enhancements in activity over a Pt/C catalyst. The authors hypothesize that the strain effect from the lattice mismatch between the shell and core components is the major determining factor for the enhancement of ORR activity and stability. Wang et al. [184] synthesized PdCo@Pd/C core–shell nanoparticles by using an H_2-induced surface segregation effect. To enhance the stability and electrocatalytic activity for the ORR, they redeposited a small number of Pt nanoparticles via a spontaneous displacement reaction and found that the Pt-deposited PdCo@Pd/C catalyst had lower OH_{ad} coverage. Thus, the lower OH_{ad} coverage on the surface of the Pt-PdCo@Pd/C catalysts improves the ORR kinetic properties. Moreover, the improvement in ORR electrocatalysis has been ascribed to many different factors, such as strain and ligand effects (responsible for the charge transfer between the components) of the core substrate [192]. Gao et al. [183] reported a new methanol-tolerant Pt/$CoSe_2$ nanobelt electrocatalyst for DMFC applications. The Pt/$CoSe_2$ nanobelt electrocatalyst was synthesized by polyol reduction (Figure 21). The transmission electron microscope (TEM) images in Figure 21(A, B) indicate that Pt nanoparticles are uniformly coated on the backbone of $CoSe_2$/ diethylenetriamine (DETA) nanobelts, and the average size of the Pt nanoparticles is ~8.3 nm (inset in Figure 21 (A)). Figure 21 (C) indicates that individual Pt nanoparticles are well dispersed on the nanobelt. The selected-area electron diffraction (SAD) pattern (inset in Figure 21 (C)) displays four rings, indexed to the (111), (200), (220), (311) planes of Pt, and also diffraction peaks of the $CoSe_2$ matrix can be detected (marked by dotted arrows). The high-resolution TEM image in Figure 21 (D) shows a lattice spacing of 19.5 nm, corresponding to that of the (220) lattice plane of a face-centered cubic Pt. The Pt/$CoSe_2$ electrocatalysts had very high ORR activity in acidic media. In addition, the Pt/$CoSe_2$ electrocatalysts are very highly resistant to methanol, even at very high concentrations (5 M).

Based on the above discussion, multiple-component catalysts not only reduce the cost but also improve the ORR activity of catalysts compared to pure Pt catalysts.

New Catalyst Supports

As mentioned above, the high cost of electrocatalysts is one of the major barriers to the commercialization of DMFCs. Therefore, many investigators have recently attempted to resolve the problem by developing new carbon-supported cathode materials. New carbon supports must have sufficient electrical conductivity so they can act as a path for the flow of electrons. In addition, new carbon supports should have a pore size range of 20–40 nm for high accessible surface area [193]. Kim et al. [194] prepared hollow core mesoporous shell (HCMS) carbon materials with different core sizes and (or) shell thicknesses and explored their use as DMFC cathode supports. According to their data analysis, HCMS carbon-supported Pt catalysts showed greater reactivity (enhancement of ~91–128% in power density)

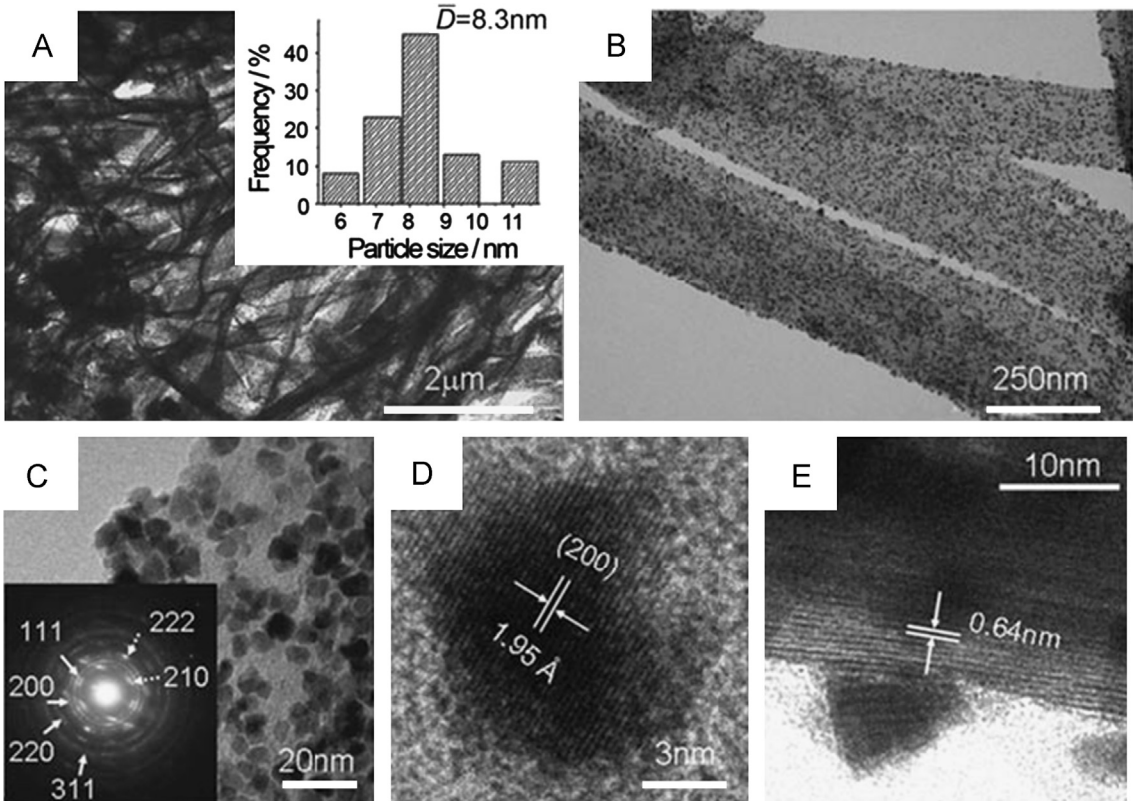

Figure 21 (A–C) TEM images of Pt/$CoSe_2$ nanobelts taken at different magnifications. The inset in (A) displays the corresponding particle size distribution histogram, and the inset in (C) displays the corresponding SAED pattern. (D) HRTEM image of a Pt nanoparticle. (E) HRTEM image along the lateral thickness direction of a Pt/$CoSe_2$ nanobelt [183]. Reprinted by permission of the Wiley-VCH Verlag GmbH & Co. KGaA.

towards the ORR than Pt/Vulcan catalysts due to the larger surface area and well-developed bimodal porosity and interstitial void channels of the HCMS carbon. They also found that the core sizes, shell thicknesses and porosities of the HCMS carbon capsules were controlled via the size of the silica sphere core, the amount and ratio of TEOS/C_{18}-TMS added, heat treatment and carbon precursors and their blends. Feng et al. [195] prepared carbon-supported $CoSe_2$ nanoparticles (non-precious metal catalyst) by an in situ surfactant-free method under mild conditions with conventional heating. Carbon-supported $CoSe_2$ nanoparticles were heated at temperatures ranging from 250 to 430 °C. The $CoSe_2$ nanoparticles have an orthorhombic (250 to 300 °C) or cubic structure (400 to 430 °C) at various temperatures in the presence of N_2. The cubic structure has higher ORR activity than the orthorhombic structure in acidic media. In addition, carbon-supported $CoSe_2$ nanoparticles have an onset potential ranging from 0.78 to 0.81 V *versus* the reference hydrogen electrode (RHE) in O_2-saturated acidic media at room temperature. Furthermore, 20 wt.% $CoSe_2$/C nanoparticles promote ~3.5 electrons per oxygen molecule during the ORR process. The authors also found the oxidation wave centered at 0.96 V *versus* RHE exhibited much higher tolerance to methanol than Pt/C. In the same year, Wang et al. [196] synthesized a highly interconnected Pt structure on noncovalently poly(diallyldimethylammonium chloride)-functionalized multiwalled carbon nanotubes (MWCNTs) via microwave-assisted polyol reduction and seed-mediated growth processes. The half-wave potential for the ORR on the 50 wt % interconnected Pt/MWCNT catalyst was 0.510 V, slightly greater than the 0.506 V observed on a conventional Pt/C catalyst. The half-wave potential value can be used to evaluate the catalytic activity of catalysts for the ORR, and more positive half-wave potentials represent enhanced catalytic activity for the ORR. Thus, the ORR activity of the interconnected Pt/MWCNTs was much better than that of conventional Pt/C catalysts. The interconnected Pt nanoparticles on MWCNTs significantly increased the number of grain boundaries, which contain the active sites for the fuel cell reactions; this increase is of considerable importance for the enhancement of ORR activity. Previous studies reported that the surface functional groups introduced into a carbon support appear to influence the ORR activity and durability of the catalysts [197]. Kou et al. [198] prepared Pt/functionalized graphene sheets (FGSs) by combined thermal expansion of graphite oxide and impregnation methods. Pt nanoparticles with an average diameter of ~2 nm were coated on FGSs. Kou et al. reported that the Pt/FGSs had high activity and much better stability in both electrochemical surface area and oxygen reduction activity than conventional catalysts due to smaller particle size and less aggregation of Pt/FGSs. Nitrogen-doped carbon nanotubes (N-CNTs) have been reported to have significant electrocatalytic activity toward the ORR in acidic and alkaline media [148,200–203]. Pt nanoparticles/N-CNTs were prepared to elucidate the role

of the N-CNT precursor solution on the morphology, nitrogen content, and resulting ORR electrocatalytic activity of Pt/N-CNT composites [203]. Pt/N-CNTs materials with ED-CNT showed the best ORR catalytic activity compared to Pt/CNT materials, which is attributed to the significant nitrogen content in composite materials (Pt/CNT with ED-CNT). Xiong et al. [204] also reported vertically aligned, nitrogen-doped carbon nanotube (VA-NCNT) arrays and applied them to study ORR activity in an acidic medium. The VA-NCNT arrays were fabricated on a cleaned Si wafer coated with a 100 nm-thick layer of silica. A mixture of Ar, H_2, and NH_3 gases of certain proportions were then used at ~850 °C in the presence of a catalyst pyrolyzing iron(II) phthalocyanine for 2 h. The VA-NCNT arrays were thus obtained. For electrochemical measurements, the prepared VA-NCNT was removed via a wet chemical method from the silica/silicon substrate and transferred onto an electrode surface. The VA-NCNT exhibited greater current output and a ~47 mV anodic shift in oxygen reduction potential relative to the Pt-black catalyst. More recently, Choi et al. [205] reported that N-CNTs grow on the outer surface of Vulcan XC-72R carbon by a pyrolysis process. Dicyandiamide (DCDA) was used an alternative precursor for N-doped carbon because it was cheap, non-flammable, and solid at room temperature. For growth of N-CNTs, DCDA was first mixed with 60 wt% Fe_2O_3 supported on Vulcan XC-72R, which acted as a catalyst for CNT growth. The mixed powder was then pyrolyzed at three different temperatures: 700, 800 and 900 °C. The samples obtained at the three different temperatures were denoted as Fe-N-C-700, Fe-N-C-800 and Fe-N-C-900. According to their data analysis, Fe-N-C-900 had the highest reactivity towards the ORR compared to Fe-N-C-700 and Fe-N-C-800, which is attributed to the N-CNTs grown on the Vulcan carbon support. As the amount of doped-N increased, the reactivity for the ORR continuously increased. Miyazaki et al. [206] studied the ORR activity of Pt nanoparticles/carbon nanospheres (Pt/CNSs), Pt nanoparticles/graphitized carbon nanospheres (GCNSs) and Pt catalyst/carbon black (CB). The ORR measurements with a rotating-ring disk electrode in an O_2-saturated H_2SO_4 aqueous solution showed that Pt/GCNS and Pt/CNS generate less H_2O_2 during oxygen reduction, compared with results obtained for Pt catalyst/CB. Further experiments indicated that the GCNSs show greater combustion tolerance and excellent electrochemical corrosion tolerance (in H_2SO_4 solution) than do CNSs and CB. Yano et al. [207] also used a similar material to that reported by the Miyazaki group. They prepared monodisperse Pt nanoparticles/graphitized CB by the nanocapsule method. The as-synthesized Pt nanoparticles/graphitized CB have higher resistance to carbon corrosion than conventional CB. Yano et al. found that Pt/graphitized CB exhibited better durability and lower H_2O_2 production rate in the potential step, cycling between 0.9 and 1.3 V. The time elapsed for the reduction of the kinetically controlled ORR mass activity to 1/2 of the initial value at Pt/graphitized CB was 30 and 60 times longer than those at the other two electrodes. They also found that the essential factors for coping with both high mass activity and high reliability are homogeneous dispersion and uniform size of Pt nanoparticles on the corrosion-resistant graphitized CB support. In 2011, Jiang et al. [208] prepared a highly active 60% Pt/C cathode electrocatalyst, which was reduced via formaldehyde and exhibited the best performance with a ~2 nm diameter. They also reported that the active surface area and dispersion of Pt nanoparticles can be controlled by the reductant and a proper amount of carbon support. By selecting both parameters, they obtained an electrocatalytic active surface area of ~66.46 m^2/g. Kim et al. [209] reported a simple synthetic route for Pt-covered MWCNTs, which are promising one-dimensional (1-D) Pt nanostructured catalysts for the ORR. The ORR activity of Pt-covered MWNTs was ~0.95 mA/cm^2 Pt at 0.9 V versus RHE, ~3-fold higher than that of a commercial catalyst Pt/C in 0.1 M $HClO_4$ electrolyte solution. The enhanced ORR activity could be attributed to the weak chemical adsorption energy of OH species on the surface of Pt-covered MWNTs. More recently, He et al. [210] synthesized polyaniline-functionalized CNTs containing Pt nanoparticles (Pt—PANI/CNTs) composites. The Pt—PANI/CNTs were initially synthesized by ethanol reduction under the protection of aniline; the CNT was well dispersed with the existence of aniline in the solution, and aniline was polymerized in the presence of a protonic acid (HCl) and ammonium persulfate (oxidizing agent). They also reported that the deposited PANI was wrapped around the CNTs as a result of π—π bonding, and well-dispersed Pt nanoparticles were coated onto the surface CNT with particle size ranging between 2.0 and 4.0 nm due to polymer stabilization and the existence of Pt—N bonding. The Pt—PANI/CNT catalysts exhibited excellent electrochemical stability due to strong binding strength between Pt and CNT walls, and PANI possesses conductivity and high stability as a conductive polymer. Based on the above discussion, we found that the obtained ORR activities and durabilities from new catalyst supports are not sufficient for use as cathode catalysts in DMFCs. Although considerable progress has been made in developing better DMFC electrode materials, the electrocatalytic properties and reliabilities of the electrodes still need to be improved.

Conclusions and future outlook

As mentioned in this review, one of the biggest challenges for our society is providing powerful electrochemical energy devices. DMFCs are amongst the most promising candidates in terms of energy density and power density. Nanostructured materials are currently of interest for such DMFCs because of their high surface areas, novel size effects, significantly enhanced kinetics, and so on. The present review describes some recent progress in the developments of nanostructured electrocatalysts for DMFCs. Approaches to reducing the cost of catalysts include the use of single—, double—, and multiple—component catalysts and new catalyst supports.

The observed DMFC performance associated with the use of single—, double—, and multiple—component catalysts and new catalyst supports has been summarized. In addition, much effort has been devoted to exploring the fundamental MOR and ORR mechanism of DMFCs. It has become evident that the unusual properties of single—, double—, and multiple—component catalysts and new support materials make them compelling for DMFC applications. The large number of research publications in the past ten years signifies the importance of fuel cells that might

surpass anode and cathode catalysts in the development of DMFCs. Challenges remain for the use of such catalysts to achieve highly efficient DMFCs. In particular, the synthetic methods, shapes, and selective catalysts of single−, double−, and multiple−component catalysts must be optimized to overcome the physical and chemical factors that limit DMFC performance. The rapid progress in the field of fuel cell catalysis will eventually allow us to use commercial DMFCs, which can supply more efficient energy to the world.

Acknowledgments

The authors gratefully acknowledge the corresponding publishers for kind permission to reproduce their materials, especially figures, for use in this review article. This work was supported by the NRF (National Honor Scientist Program: 2010−0020414, WCU: R32−2008−000−10180−0.

References

[1] C.C. Yang, C.T. Lin, S.J. Chiu, Desalination 233 (2008) 137.
[2] E.A. Carbonio, F. Colmati, E.G. Ciapina, M.E. Pereira, E. R. Gonzalez, Journal of the Brazilian Chemical Society. 21 (2010) 590.
[3] C.J. Zhong, J. Luo, B. Fang, B.N. Wanjala, P.N. Njoki, R. Loukrakpam, J. Yin, Nanotechnology 21 (2010) 062001.
[4] V. Mazumder, Y. Lee, S. Sun, Advanced Functional Materials 20 (2010) 1224.
[5] D.S. Su, R. Schlçgl, ChemSusChem 3 (2010) 136.
[6] Y.G. Guo, J.S. Hu, L.J. Wan, Advanced Materials 20 (2008) 2878.
[7] A. Manthiram, A.V. Murugan, A. Sarkar, T. Muraliganth, Energy and Environmental Science 1 (2008) 621.
[8] E.H. Yu, U. Krewer, K. Scott, Energies 3 (2010) 1499.
[9] F. Vigier, S. Rousseau, C. Coutanceau, J.M. Leger, C. Lamy, Topics in Catalysis. 40 (2006) 111.
[10] K. Kordesch, G. Simader, Fuel Cells and Their Applications, VCH Publishing, Weinheim, 1996.
[11] G.B. Jung, et al., Journal of Solid State Electrochemistry 13 (2009) 1455.
[12] O. Zerbinati, A. Mardan, M.M. Richter, Journal of Chemical Education 79 (2002) 829.
[13] A. Manthiram, The WSTIAC Quarterly 9 (2009) 69.
[14] A.S. Aricò, V. Baglio, V. Antonucci, Direct Methanol Fuel Cells: History, Status and Perspectives 1 (2009) (Chapter 1).
[15] Y.L. Liu, Y.H. Su, C.M. Chang, Suryani, D.M. Wang, J.Y. Lai, Journal of Materials Chemistry 20 (2010) 4409.
[16] N.A. Hampson, M.J. Willars, B.D. McNicol, Journal of Power Sources 4 (1979) 191.
[17] D.S. Cameron, G.A. Hards and D. Thompsett, in: Proceedings of the Workshop on Direct Methanol-Air Fuel Cell, 1990, p. 10.
[18] A. Hamnett, Catalysis Today 38 (1997) 445.
[19] R. Parsons, T. Vander Noot, Journal of Electroanalytical Chemistry 257 (1988) 9.
[20] C. Lamy, J.M. Leger, S. Srinivasan, in: J.O.'M. Bockris, B. E. Conway, R.E. White (Eds.), Modern Aspects of Electrochemistry, 34, 2001, p. 53.
[21] C. Song, J Zhang 2, Electrocatalytic oxygen reduction reaction, in: J. Zhang (Ed.), PEM Fuel Cell Electrocatalysts and Catalyst Layers: Fundamentals and ApplicationsSpringer, 2008, pp. 89-134.
[22] Z. Xu, H. Li, G. Cao, Q. Zhang, K. Li, X. Zhao, Journal of Molecular Catalysis A: Chemical 335 (2011) 89.
[23] F. Mirkhalaf, K. Tammeveskic, D.J. Schiffrina, Physical Chemistry Chemical Physics 11 (2009) 3463.
[24] E. Antolini, Energy and Environmental Science 2 (2009) 915.
[25] E. Antolini, J. Perez, Journal of Materials Science 46 (2011) 4435.
[26] Y. Lu, J. Tu, C. Gu, X. Xia, X. Wang, S.X. Mao, Journal of Materials Chemistry 21 (2011) 4843.
[27] V. Mazumder, Y. Lee, S. Sun, Advanced Functional Materials 20 (2010) 1224.
[28] Z. Borkowska, A. Tymosiak-Zielinska, G. Shul, Electrochimica Acta 49 (2004) 1209.
[29] G. Tremiliosi-Filho, E.R. Gonzalez, A.J. Motheo, E.M. Belgsir, J.M. Leger, C. Lamy, Journal of Electroanalytical Chemistry 444 (1998) 31.
[30] J. Zhang, P. Liu, H. Ma, Y. Ding, Journal of Physical Chemistry C 111 (2007) 10382.
[31] W. Li, H. Ma, J. Zhang, X. Liu, X. Feng, Journal of Physical Chemistry C 113 (2009) 1738.
[32] X. Wang, W. Wang, Z. Qi, C. Zhao, H. Ji, Z. Zhang, Journal of Power Sources 195 (2010) 6740.
[33] J.N. Tiwari, F.M. Pan, K.L. Lin, New Journal of Chemistry 33 (2009) 1482.
[34] Y.B. He, G.R. Li, Z.L. Wang, Y.N. Ou, Y.X. Tong, Journal of Physical Chemistry C 114 (2010) 19175.
[35] J. Solla-Gullon, F.J. Vidal-Iglesias, A. Lopez-Cudero, E. Garnier, J.M. Feliu, A. Aldaz, Physical Chemistry Chemical Physics 10 (2008) 3689.
[36] S.B. Han, Y.J. Song, J.M. Lee, J.Y. Kim, K.W. Park, Electrochemistry Communications 10 (2008) 1044.
[37] Y.W. Lee, S.B. Han, D.Y. Kim, K.W. Park, Chemical Communications 47 (2011) 6296.
[38] J.N. Tiwari, R.N. Tiwari, K.L. Lin, Nano Research 4 (2011) 541.
[39] S.M. Alia, G. Zhang, D. Kisailus, D. Li, S. Gu, K. Jensen, Y. Yan, Advanced Functional Materials 20 (2010) 3742.
[40] J.N. Tiwari, F.M. Pan, R.N. Tiwari, S.K. Nandi, Chemical Communications 48 (2008) 6516.
[41] H.P. Liang, H.M. Zhang, J.S. Hu, Y.G. Guo, L.J. Wan, C.L. Bai, Angewandte Chemie International Edition 43 (2004) 1540.
[42] M. Rauber, I. Alber, S. Muller, R. Neumann, O. Picht, C. Roth, A. Schokel, M.E. Toimil-Molares, W. Ensinger, Nano Letters 11 (2011) 2304.
[43] G. Stalnionis, L. Tamasauskaite-Tamasiunaite, V. Pautieniene, A. Sudavicius, Z. Jusys, Journal of Solid State Electrochemistry 8 (2004) 892.
[44] B. Gurau, R. Viswanathan, R. Liu, T.J. Lafrenz, K.L. Ley, E. S. Smotkin, E. Reddington, A. Sapienza, B.C. Chan, T. E. Mallouk, S. Sarangapani, Journal of Physical Chemistry B 102 (1998) 9997.
[45] T. Yajima, H. Uchida, M. Watanabe, Journal of Physical Chemistry B 108 (2004) 2654.
[46] Y.H. Lin, X.L. Cui, Langmuir 21 (2005) 11474.
[47] E.P. Ambrosio, C. Francia, M. Manzoli, P. Nerino, International Journal of Hydrogen Energy 33 (2008) 3142.
[48] J. Zeng, J.Y. Lee, Journal of Power Sources 140 (2005) 268.
[49] Y.I. Kim, D. Soundararajan, C.W. Park, S.H. Kim, J.H. Park, J. M. Ko, International Journal of Hydrogen Energy 4 (2009) 1548.
[50] T. Maiyalagan, International Journal of Hydrogen Energy 34 (2009) 2874.
[51] S.J. Yoo, T.Y. Jeon, K.S. Kim, T.H. Lima, Y.E. Sung, Physical Chemistry Chemical Physics 12 (2010) 15240.
[52] A.O. Neto, R.R. Dias, M.M. Tusi, M. Linardi, E.V. Spinacé, Journal of Power Sources 166 (2007) 87.
[53] H.B. Hassan, Journal of Fuel Chemistry and Technology 37 (2009) 346.
[54] Z. Qi, et al., Journal of Power Sources 196 (2011) 5823.
[55] S.A. Lee, K.W. Park, J.H. Choi, B.K. Kwon, Y.E. Sung, Journal of the Electrochemical Society 149 (2002) A1299.

[56] T.Y. Morante-Catacora, Y. Ishikawa, C.R. Cabrera, Journal of Electroanalytical Chemistry 621 (2008) 103.
[57] C.S. Chen, F.M. Pan, Applied Catalysis B: Environmental 91 (2009) 663.
[58] L. Xing, J. Jia, Y. Wang, B. Zhang, S. Dong, International Journal of Hydrogen Energy 35 (2010) 12169.
[60] J. Huang, H. Yang, Q. Huang, Y. Tang, T. Lu, D.L. Akins, Journal of the Electrochemical Society 151 (2004) A1810.
[61] Y. Kang, C.B. Murray, Journal of the American Chemical Society 132 (2010) 7568.
[62] J. Zhang, H. Ma, D. Zhang, P. Liu, F. Tian, Y. Ding, Physical Chemistry Chemical Physics 10 (2008) 3250.
[63] Y.Q. Wang, Z.D. Wei, L. Li, M.B. Ji, Y. Xu, P.K. Shen, J. Zhang, H. Zhang, Journal of Physical Chemistry C 112 (2008) 18672.
[64] Z. Zhang, Y. Wang, X. Wang, Nanoscale 3 (2011) 1663.
[65] Y.W. Lee, A.R. Ko, S.B. Han, H.S. Kim, K.W. Park, Physical Chemistry Chemical Physics 13 (2011) 5569.
[66] F. Kadirgan, S. Beyban, T. Atilan, International Journal of Hydrogen Energy 34 (2009) 4312.
[67] Q. Jiang, L. Jiang, H. Hou, J. Qi, S. Wang, G. Sun, Journal of Physical Chemistry C 114 (2010) 19714.
[68] S.Y. Shen, T.S. Zhao, J.B. Xu, Y.S. Li, Journal of Power Sources 195 (2010) 1001.
[69] N.V. Long, T.D. Hien, T. Asaka, M. Ohtaki, M. Nogami, International Journal of Hydrogen Energy 36 (2011) 8478.
[70] M. Khalid, N. Wasio, T. Chase, K. Bandyopadhyay, Nanoscale Research Letters 5 (2010) 61.
[71] D.I. Garcia-Gutierrez, C.E. Gutierrez-Wing, L. Giovanetti, J. M. Ramallo-Lopez, F.G. Requejo, M. Jose-Yacaman, Journal of Physical Chemistry B 109 (2005) 3813.
[73] T. Ghosh, Q. Zhou, J.M. Gregoire, R.B. Dover, F.J. DiSalvo, Journal of Physical Chemistry C 114 (2010) 12545.
[74] X. Shi, X. Jin, W. Xiao, X. Hou, H. Chen, G.Z. Chen, Chemistry —A European Journal 17 (2011) 8562.
[76] L. Wang, Y. Nemoto, Y. Yamauchi, Journal of the American Chemical Society 133 (2011) 9674.
[77] C.H. Cui, H.H. Li, S.H. Yu, Chemical Science 2 (2011) 1611.
[78] M.K. Min, J. Cho, K. Cho, H. Kim, Electrochimica Acta 45 (2000) 4211.
[80] H. Yang, J. Zhang, K. Sun, S. Zou, J. Fang, Angewandte Chemie International Edition 49 (2010) 6848.
[81] M. Watanabe, S. Motoo, Journal of Electroanalytical Chemistry 60 (1975) 267.
[82] J.A.R. Van Veen, T. Frelink, W. Visscher, Surface Science. 335 (1995) 353.
[83] X. Peng, K. Koczkur, A. Chen, Nanotechnology 18 (2007) 305605.
[85] S. Şen, F. Şen, G. Gökağaç, Physical Chemistry Chemical Physics 13 (2011) 6784.
[86] C. Ma, Z. Chen, F. Zhao, Chinese Journal of Chemistry. 29 (2011) 611.
[87] M.Y. Wang, J.H. Chen, K.Z. Cui, B. Liu, H.H. Zhou, Y.F. Kuang, Chinese Journal of Chemistry. 24 (2006) 881.
[88] M.V. Martínez-Huerta, S. Rojas, J.L. Gómez de la Fuente, P. Terreros, M.A. Peña, J.L.G. Fierro, Applied Catalysis B: Environmental. 69 (2006) 75.
[89] S. Pasupathi, V. Tricoli, Journal of Solid State Electrochemistry. 12 (2007) 1093.
[90] T. Huang, J. Liu, R. Li, W. Cai, A. Yu, Electrochemistry Communications 11 (2009) 643.
[91] A. Oliveira Neto, E.G. Franco, E. Aricó, M. Linardi, Portugaliae Electrochimica Acta 22 (2004) 93.
[92] Z.B. Wang, P.J. Zuo, G.P. Yin, Fuel Cells 9 (2009) 106.
[93] T. Maiyalagan, B. Viswanathan, U.V. Varadaraju, Journal of Nanoscience and Nanotechnology 6 (2006) 2067.
[94] T. Maiyalagan, B. Viswanathan, Journal of Power Sources 175 (2008) 789.
[95] T. Maiyalagan, F.N. Khan, Catalysis Communications 10 (2009) 433.
[96] C. Zhou, H. Wang, F. Peng, J. Liang, H. Yu, J. Yang, Langmuir 25 (2009) 7711.
[97] G.S. Chai, J.S. Yu, Journal of Materials Chemistry 19 (2009) 6842.
[98] S. Sun, G. Zhang, D. Geng, Y. Chen, M.N. Banis, R. Li, M. Cai, X. Sun, Chemistry—A European Journal 16 (2010) 829.
[99] Z. Sun, X. Wang, Z. Liu, H. Zhang, P. Yu, L. Mao, Langmuir 26 (2010) 12383.
[100] S. Yamazaki, M. Yao, Z. Siroma, T. Ioroi, K. Yasuda, Journal of Physical Chemistry C 114 (2010) 21856.
[101] S.S. Kim, C. Kim, H. Lee, Topics in Catalysis. 53 (2010) 686.
[102] S.H. Ahn, O.J. Kwon, S.K. Kim, I. Choi, J.J. Kim, International Journal of Hydrogen Energy 35 (2010) 13309.
[103] A. Sarkar, A. Vadivel Murugan, A. Manthiram, Fuel Cells 10 (2010) 375.
[104] T. Saida, N. Ogiwara, Y. Takasu, W. Sugimoto, Journal of Physical Chemistry C 114 (2010) 13390.
[105] M.K. Jeon, K.R. Lee, S.I. Woo, Langmuir 26 (2010) 16529.
[106] K.I.B. Eguiluz, G.R.P. Malpass, M.M.S. Pupo, G.R. Salazar-Banda, L.A. Avaca, Energy Fuels 24 (2010) 4012.
[107] S. Li, X. Yu, G. Zhang, Y. Ma, J. Yao, P. Oliveira, Carbon 49 (2011) 1906.
[108] J. Wu, Y. Hou, S. Gao, Nano Research. 4 (2011) 836.
[109] C. Pan, Y. Li, Y. Ma, X. Zhao, Q. Zhang, Journal of Power Sources 196 (2011) 6228.
[110] L. Liu, Z. Huang, D. Wang, R. Scholz, E. Pippel, Nanotechnology 22 (2011) 105604.
[111] ⟨http://www.kitco.com/charts/liveplatinum.html⟩ (retrieved 30.07.09).
[112] H. Chang, S.H. Joo, C. Pak, Journal of Materials Chemistry 17 (2007) 3078.
[113] G.S. Chai, S.B. Yoon, J.H. Kim, J.S. Yu, Chemical Communications 2766 (2004).
[114] R. Ganesan, J.S. Lee, Angewandte Chemie International Edition 44 (2005) 6557.
[115] S. Shanmugam, A. Gedanken, Small 3 (2007) 1189.
[116] S.H. Joo, et al., Carbon 46 (2008) 2034.
[119] C.T. Hsieh, J.Y. Lin, Journal of Power Sources 188 (2009) 347.
[120] Y. Ding, B. Jin, G. Gu, X.H. Xia, Journal of Materials Chemistry 19 (2009) 9141.
[121] J.N. Tiwari, R.N. Tiwari, Y.M. Chang, K.L. Lin, ChemSusChem 3 (2010) 460.
[122] J.B. Joo, N.D. Kim, H.J. Yun, P. Kim, J. Yi, Nano Research 4 (2011) 92.
[123] S. Sharma, A. Ganguly, P. Papakonstantinou, X. Miao, M. Li, J. L. Hutchison, M. Delichatsios, S. Ukleja, Journal of Physical Chemistry C 114 (2010) 19459.
[124] Y. Ou, X. Cui, X. Zhang, Z. Jiang, Journal of Power Sources 195 (2010) 1365.
[125] J.N. Tiwari, F.M. Pan, T.M. Chen, R.N. Tiwari, K.L. Lin, Journal of Power Sources 195 (2010) 729.
[126] J.N. Tiwari, R.N. Tiwari, K.L. Lin, ACS Applied Materials and Interfaces 2 (2010) 2231.
[127] W.C. Fang, Nanoscale Research Letters 5 (2010) 68.
[128] J.S. Bunch, et al., Science 315 (2007) 490.
[129] A.K. Geim, K.S. Novoselov, Nature Materials 6 (2007) 183.
[130] S. Park, R.S. Ruoff, Nature Nanotechnology. 4 (2009) 217.
[131] J.N. Tiwari, R.N. Tiwari, G. Singh, K.L. Lin, Plasmonics 6 (2011) 67.
[132] Y.G. Zhou, J.J. Chen, F. Wang, Z.H. Sheng, X.H. Xia, Chemical Communications 5951 (2010).
[133] S. Guo, S. Dong, E. Wang, ACS Nano 4 (2010) 547.
[135] Y. Zhang, et al., Chemistry—A European Journal 17 (2011) 4921.
[136] S. Shanmugam, A. Gedanken, Journal of Physical Chemistry C 113 (2009) 18707.
[137] J.K. Oh, et al., Catalysis Science and Technology 1 (2011) 394.

[138] L. Kuai, B. Geng, S. Wang, Y. Zhao, Y. Luo, H. Jiang, Chemistry—A European Journal 17 (2011) 3482.
[139] C. Jeyabharathi, S.S. Kumar, G.V.M. Kiruthika, K.L.N. Phani, Angewandte Chemie International Edition 49 (2010) 2925.
[140] L. Johnson, W. Thielemans, D.A. Walsh, Green Chemistry (2011). http://dx.doi.org/10.1039/c0gc00881h.
[141] G.F. A´lvarez, M. Mamlouk, K. Scott, International Journal of Electrochemistry (2011). http://dx.doi.org/10.4061/2011/684535.
[142] H. Li, Q. Xin, W. Li, Z. Zhou, L. Jiang, S. Yang, G. Sun, Chemical Communications 2776 (2004).
[143] R. Liu, D. Wu, X. Feng, K. Mullen, Angewandte Chemie International Edition 49 (2010) 2565.
[144] S. Yang, X. Feng, X. Wang, K. Mullen, Angewandte Chemie International Edition 50 (2011) 5339.
[145] D. Xia, S. Liu, Z. Wang, G. Chen, L. Zhang, L. Zhang, S. Hui, J. Zhang, Journal of Power Sources 177 (2008) 296.
[146] T.C. Nagaiah, S. Kundu, M. Bron, M. Muhler, W. Schuhmann, Electrochemistry Communications 12 (2010) 338.
[147] W.Z. Li, C.H. Liang, J.S. Qiu, Carbon 40 (2002) 791.
[148] K. Gong, F. Du, Z. Xia, M. Durstock, L. Dai, Science 323 (2009) 760.
[149] S.S. Roy, P. Papakonstantinou, T.I.T. Okpalugo, H. Murphy, Journal of Applied Physics 100 (2006) 053703.
[150] J.I. Ozaki, S.I. Tanifuji, N. Kimura, A. Furuichi, A. Oya, Carbon 44 (2006) 1324.
[151] S. Maldonado, K.J. Stevenson, Journal of Physical Chemistry B 109 (2005) 4707.
[152] F. Wen, U. Simon, Chemistry of Materials 19 (2007) 3370.
[153] C. Wang, H. Daimon, T. Onodera, T. Koda, S. Sun, Angewandte Chemie International Edition 47 (2008) 3588.
[154] T. Yu, D.Y. Kim, H. Zhang, Y. Xia, Angewandte Chemie International Edition 50 (2011) 2773.
[155] S.H. Sun, F. Jaouen, J.P. Dodelet, Advanced Materials 20 (2008) 3900.
[156] E.P. Lee, Z.M. Peng, W. Chen, S.W. Chen, H. Yang, Y.N. Xia, ACS Nano 2 (2008) 2167.
[157] H.J. Zhou, W.P. Zhou, R.R. Adzic, S.S. Wong, Journal of Physical Chemistry C 113 (2009) 5460.
[158] H.W. Liang, X. Cao, F. Zhou, C.H. Cui, W.J. Zhang, S.H. Yu, Advanced Materials 23 (2011) 1467.
[159] H.H. Wang, Z.Y. Zhou, Q. Yuan, N. Tian, S.G. Sun, Chemical Communications 3407 (2011).
[161] Y. Bing, H. Liu, L. Zhang, D. Ghosh, J. Zhang, Chemical Society Reviews 39 (2010) 2184.
[162] C.J. Yang, Energy Policy 37 (2009) 1805.
[163] Y.X. Wang, P.B. Balbuena, Journal of Physical Chemistry B 109 (2005) 18902.
[165] A. Sarkar, A. Vadivel Murugan, A. Manthiram, Journal of Materials Chemistry 19 (2009) 159.
[166] P.H.C. Camargo, Z. Peng, X. Lu, H. Yang, Y. Xia, Journal of Materials Chemistry 19 (2009) 1024.
[167] H. Liu, A. Manthiram, Energy and Environmental Science 2 (2009) 124.
[168] A.M. Remona, K.L.N. Phani, Fuel Cells 11 (2011) 385.
[169] F.J. Lai, W.N. Su, L.S. Sarma, D.G. Liu, C.A. Hsieh, J.F. Lee, B.J. Hwang, Chemistry—A European Journal 16 (2010) 4602.
[170] S.H. Chang, W.N. Su, M.H. Yeh, C.J. Pan, K.L. Yu, D.G. Liu, J. F. Lee, B.J. Hwang, Chemistry—A European Journal 16 (2010) 11064.
[171] W. Li, Q. Xin, Y. Yan, International Journal of Hydrogen Energy 35 (2010) 2530.
[172] P.H. Fernndez, S. Rojas, P. Ocon, J.L.G. Fuente, J.S. Fabian, J. Sanza, et al., Journal of Physical Chemistry C 111 (2007) 2913.
[173] J. Zhang, K. Sasaki, E. Sutter, R.R. Adzic, Science 315 (2007) 220.
[174] J.B. Xu, T.S. Zhao, W.W. Yang, S.Y. Shen, International Journal of Hydrogen Energy 35 (2010) 8699.
[175] Y. Kim, J.W. Hong, Y.W. Lee, M. Kim, D. Kim, W.S. Yun, S. W. Han, Angewandte Chemie International Edition 49 (2010) 10197.
[176] I. Dutta, M.K. Carpenter, M.P. Balogh, J.M. Ziegelbauer, T. E. Moylan, M.H. Atwan, N.P. Irish, Journal of Physical Chemistry C 114 (2010) 16309.
[177] K.M. Yeo, S. Choi, R.M. Anisur, J. Kim, I.S. Lee, Angewandte Chemie International Edition 50 (2011) 745.
[178] Z. Chen, M. Waje, W. Li, Y. Yan, Angewandte Chemie International Edition 46 (2007) 4060.
[179] Z. Zhang, M. Li, Z. Wu, W. Li, Nanotechnology 22 (2011) 015602.
[180] T. Fujigaya, T. Uchinoumi, K. Kaneko, N. Nakashima, Chemical Communications 6843 (2011).
[181] T. He, E. Kreidler, Physical Chemistry Chemical Physics 10 (2008) 3731.
[182] R. Srivastava, P. Mani, N. Hahn, P. Strasser, Angewandte Chemie International Edition 46 (2007) 8988.
[183] M.R. Gao, Q. Gao, J. Jiang, C.H. Cui, W.T. Yao, S.H. Yu, Angewandte Chemie International Edition 50 (2011) 4905.
[184] D. Wang, et al., Journal of the American Chemical Society 132 (2010) 17664.
[185] W. Zhang, R. Wang, H. Wang, Z. Lei, Fuel Cells 10 (2010) 734.
[186] R. Loukrakpam, et al., ACS Catalysis 1 (2011) 562.
[187] V. Mazumder, M. Chi, K.L. More, S. Sun, Journal of the American Chemical Society 132 (2010) 7848.
[188] D. Wang, et al., Journal of the American Chemical Society 132 (2010) 10218.
[190] L. Liu, E. Pippel, Angewandte Chemie International Edition 50 (2011) 2729.
[191] J. Yang, C.H. Cheng, W. Zhou, J.Y. Lee, Z. Liu, Fuel Cells 10 (2010) 907.
[192] V.R. Stamenkovic, B.S. Mun, K.J.J. Mayrhofer, P.N. Ross, N. M. Markovic, Journal of the American Chemical Society 128 (2006) 8813.
[193] E.r.m.e.t.e. Antolini, Applied Catalysis B: Environmental 88 (2009) 1.
[194] J.H. Kim, B. Fang, S.B. Yoon, J.S. Yu, Applied Catalysis B: Environmental 88 (2009) 368.
[195] Y.J. Feng, T. He, N. Alonso-Vante, Fuel Cells 10 (2010) 77.
[196] S. Wang, S.P. Jiang, T.J. White, J. Guo, X. Wang, Journal of Physical Chemistry C 113 (2009) 18935.
[197] Y.C. Xing, L. Li, C.C. Chusuei, R.V. Hull, Langmuir 21 (2005) 4185.
[198] R. Kou, et al., Electrochemistry Communications 11 (2009) 954.
[200] G. Vijayaraghavan, K. Stevenson, Langmuir 23 (2007) 5279.
[201] Y. Chen, J. Wang, H. Liu, R. Li, X. Sun, S. Ye, S. Knights, Electrochemistry Communications 11 (2009) 2071.
[202] M. Saha, R. Li, X. Sun, S. Ye, Electrochemistry Communications 11 (2009) 438.
[203] D.C. Higgins, D. Meza, Z. Chen, Journal of Physical Chemistry C 114 (2010) 21982.
[204] W. Xiong, et al., Journal of the American Chemical Society 132 (2010) 15839.
[205] C.H. Choi, S.Y. Lee, S.H. Park, S.I. Woo, Applied Catalysis B: Environmental 103 (2011) 362.
[206] K. Miyazaki, H. Shirakata, T. Abe, N. Yoshizawa, Z. Ogumi, Fuel Cells 10 (2010) 960.
[207] H. Yano, T. Akiyama, P. Bele, H. Uchida, M. Watanabe, Physical Chemistry Chemical Physics 12 (2010) 3806.
[208] Q. Jiang, Z. Peng, X. Xie, K. Du, G. Hu, Y. Liu, Transactions of Nonferrous Metals Society of China 21 (2011) 127.
[209] J. Kim, S.W. Lee, C. Carlton, Y. Shao-Horn, Journal of Physical Chemistry Letters 2 (2011) 1332.
[210] D. He, C. Zeng, C. Xu, N. Cheng, H. Li, S. Mu, M. Pan, Langmuir 27 (2011) 5582.

Jitendra N. Tiwari received his Ph.D. degree in electrochemistry from the Department of Materials Science and Engineering, National Chiao Tung University, Taiwan in 2009 working on synthesis of highly durable catalysts for electrochemical energy devices. He was a postdoctoral research fellow at the Institute of Nanotechnology, National Chiao Tung University, Taiwan (August 2009-July 2010). Currently, he is a postdoctoral research scientist at the Department of Chemistry, Pohang University of Science and Technology and focuses on graphene-based materials for fuel cell applications.

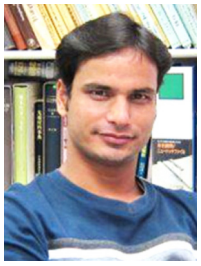

Rajanish N. Tiwari was born in India. He received his B.S. and M.S. from H. N. B. Garhwal University, India, and a Ph.D. degree in Materials Science and Engineering from National Chiao Tung University, Taiwan in 2010. Currently, he is working in Japan as a postdoctoral fellow at Toyota Technological Institute. His postdoctoral fellowship funded by Toyota Motor Corporation. His current interests include study of the synthesis, characterization, and application of novel carbon materials. He has published many scientific papers in refereed journals and given presentations.

Gyan Singh was born in 1984 in Bihar, India. He earned his B.Sc. (Hons.) in Biochemistry from Allahabad Agricultural Institute –Deemed University, India, in 2006. In the same year he was awarded Taiwan Government Fellowship to pursue Master of Science (MS) in Molecular Medicine and Bioengineering from National Chaio Tung University, Taiwan. Currently he is perusing his Doctoral research under supervision of Prof. Yun-Ming Wang at National Chaio Tung University. His primary research interests include design and development of nanosensors for clinically relevant biomolecules.

Kwang S. Kim received his Ph.D. degree from University of California, Berkeley. He was a postdoctoral fellow at IBM and a visiting professor or scientist at Rutgers University, MIT, and Columbia University. Currently, he is a professor in the Department of Chemistry and the director of the Center for Superfunctional Materials at Pohang University of Science and Technology. His research interests include design and development of novel nanomaterials and molecular devices.